CANCER

CD4$^+$FOXP3Exon2$^+$ regulatory T cell frequency predicts breast cancer prognosis and survival

Clorinda Fusco[1]†, Francesca Di Rella[2]†, Antonietta Liotti[3,4]†, Alessandra Colamatteo[1], Anne Lise Ferrara[4], Vincenzo Gigantino[5], Francesca Collina[5], Emanuela Esposito[6], Ivana Donzelli[6], Antonio Porcellini[7], Antonia Feola[7], Teresa Micillo[1], Francesco Perna[8], Federica Garziano[9], Giorgia Teresa Maniscalco[10], Gilda Varricchi[3,4], Maria Mottola[11], Bruno Zuccarelli[11], Bruna De Simone[12], Maurizio di Bonito[5], Giuseppe Matarese[1,3], Antonello Accurso[13], Martina Pontillo[13], Daniela Russo[14], Luigi Insabato[14], Alessandra Spaziano[1], Irene Cantone[1,3]*‡, Antonio Pezone[7]*‡, Veronica De Rosa[3]*‡

CD4$^+$FOXP3$^+$ regulatory T cells (T_{regs}) suppress immune responses to tumors, and their accumulation in the tumor microenvironment (TME) correlates with poor clinical outcome in several cancers, including breast cancer (BC). However, the properties of intratumoral T_{regs} remain largely unknown. Here, we found that a functionally distinct subpopulation of T_{regs}, expressing the FOXP3 Exon2 splicing variants, is prominent in patients with hormone receptor–positive BC with poor prognosis. Notably, a comprehensive examination of the TCGA validated FOXP3E2 as an independent prognostic marker in all other BC subtypes. We found that FOXP3E2 expression underlies BCs with defective mismatch repair and a stem-like signature and highlights pathways involved in tumor survival. Last, we found that the TME induces FOXP3E2 through the CXCL12/CXCR4 axis and confirmed the higher immunosuppressive capacity of FOXP3E2$^+$ T_{regs} derived from patients with BC. Our study suggests that FOXP3E2$^+$ T_{regs} might be used as an independent biomarker to predict BC prognosis and survival and to develop super-targeted immunotherapies.

INTRODUCTION

Immune surveillance against cancer is an important strategy for tracing, identifying, and eliminating growing tumor cells (*1*–*4*). Nonetheless, the immune system can shape tumor genomes by selecting neoantigen-depleted clones (i.e., immune editing) or promoting the accumulation of clones with an immune evasion strategy (i.e., immune escape), representing one of the main drivers of relapse (*5*, *6*). Breast cancer (BC) is more resistant to immunotherapies than other solid tumors (*7*, *8*), with a large window of recurrence spanning from months to decades after surgery (*9*, *10*). Although the exact cause of this unusual recurrence pattern is still unknown, patients with luminal cancer typically have a better prognosis, whereas basal-like and human epidermal growth factor receptor 2 (HER2)–enriched patients experience early relapses (within the first 5 years after diagnosis) (*11*, *12*). However, the risk of late recurrence ranges from 10 to 41% in all BC subgroups, based on their primary tumor classification system [e.g., tumor-node-metastasis (TNM)] (*13*), population-based data, and occasionally primary tumor gene expression profiles (*14*). Although the highest cumulative incidence has been observed among estrogen receptor (ER)–positive patients, late recurrences also occur among those with ER-negative tumors (*15*, *16*). It is, therefore, of paramount importance to identify prognostic biomarkers alongside with the causes of recurrence (*17*).

The interaction between tumor, stromal, and immune cells may promote metastatic progression and immune escape, challenging cancer immunotherapy efficacy (*5*, *18*). Antitumor-specific T cell responses arise in patients with BC but are halted by suppressive mechanisms established in the TME during tumor progression (*19*). CD4$^+$CD25$^+$ regulatory T cells (T_{regs}) expressing the Forkhead-box-p3 (FOXP3) transcription factor are enriched in the tumor microenvironment (TME) and associate with an invasive phenotype as well as reduced relapse-free and overall survival in several cancers (*20*), consistent with their role in suppressing effector cells. Transient depletion of T_{regs} via CD25, CTLA4, or CCR4 blockade results in improved clinical outcomes and increased antitumor-specific immune responses (*19*). FOXP3$^+$ T_{regs} variably infiltrate human BC and mainly correlate with reduced survival and poor prognosis (*1*, *21*–*26*). Although their central function in tumor escape (*27*) and their role as therapeutic targets of immune checkpoint (IC) inhibitors, the properties of intratumoral T_{regs} remain largely unknown, and they are not a good prognostic marker for BC (*23*, *28*). Published transcriptomic profiles indicate that tumor-infiltrating T_{regs} constitute a heterogeneous population (*29*, *30*). Whether the tumor milieu imprints unique functional and transcriptional features to T_{regs} or whether

[1]Dipartimento di Medicina Molecolare e Biotecnologie Mediche, Università degli Studi di Napoli "Federico II", Napoli, Italy. [2]Oncologia Clinica Sperimentale di Senologia, Istituto Nazionale Tumori, IRCCS, Fondazione Pascale, Napoli, Italy. [3]Istituto per l'Endocrinologia e l'Oncologia Sperimentale "G. Salvatore", IEOS-CNR, Napoli, Italy. [4]Dipartimento di Scienze Mediche Traslazionali, Università degli Studi di Napoli "Federico II", Napoli 80131, Italy. [5]Unità di Anatomia Patologica, Istituto Nazionale Tumori, IRCCS, Fondazione Pascale, Napoli, Italy. [6]Chirurgia Oncologica di Senologia, Istituto Nazionale Tumori, IRCCS, Fondazione Pascale, Napoli, Italy. [7]Dipartimento di Biologia, Complesso Universitario di Monte Sant'Angelo, Università di Napoli "Federico II", Napoli 80126, Italy. [8]Dipartimento di Medicina Clinica e Chirurgia, Università degli Studi di Napoli "Federico II", Napoli 80131, Italy. [9]U.O.C Biochimica Clinica Azienda Ospedaliera Specialistica dei Colli Monaldi-Cotugno-C.T.O. Presidio Monaldi, Napoli, Italy. [10]Clinica Neurologica e Unità Stroke, Centro Sclerosi Multipla, Ospedale "A.Cardarelli", Napoli 80131, Italy. [11]U.O.C Medicina Trasfusionale, Azienda Ospedaliera Specialistica dei Colli, Napoli 80131, Italy. [12]Dipartimento di Sanità Pubblica, Università degli Studi di Napoli "Federico II", Napoli 80131, Italy. [13]Dipartimento di Chirurgia Generale, Oncologica, Bariatrica e Metabolica, Università degli Studi di Napoli "Federico II", Napoli 80131, Italy. [14]Unità di Anatomia Patologica, Dipartimento di Scienze Biomediche Avanzate, Facoltà di Medicina, Università degli Studi di Napoli "Federico II", Napoli 80131, Italy.
*Corresponding author. Email: veronica.derosa@cnr.it (V.D.R.); antonio.pezone@unina.it (A.Pe.); irene.cantone@unina.it (I.C.)
†These authors contributed equally to this work.
‡These authors contributed equally to this work.

distinct subsets of peripheral blood (PB) T_{regs} are differentially recruited within the tumor is still unclear (*31*, *32*). Characterizing tumor-infiltrating T_{regs} will, therefore, be key to find biomarkers and develop therapies that precisely target cells that block antitumor response without altering peripheral self-tolerance.

In humans, the master regulator of T_{reg} development and function is *FOXP3* gene. It comprises 12 exons encoding multiple transcript variants, among which four are co-expressed at different levels in circulating T_{regs}, including the full-length (FOXP3FL) and those lacking Exon2 (FOXP3Δ2), which are generally more abundant (*33*, *34*). Several reports uncover indispensable functions of the 105–base pair region constituting *FOXP3 Exon2* (*FOXPE2*), thus highlighting a possible role for this region in regulating a transcriptional program that maintains T_{reg} stability and immune homeostasis (*34*–*37*). In patients with autoimmunity, we reported a selective reduction of FOXP3E2 splicing variants associated with impaired T_{reg} suppressive function (*35*). Here, we study the distribution and function of FOXP3E2$^+$ T_{regs}, both in the TME and PB of patients with BC to explore their connection with the molecular landscape of the primary tumor and patient prognosis.

RESULTS

FOXP3E2$^+$ T_{regs} are enriched in the tumor infiltrate and PB of patients with HR$^+$ BC

High infiltration of FOXP3$^+$ T_{regs} is expected to be associated with an unfavorable outcome in several cancers, but studies of BC have led to highly discrepant findings (*38*). Here, we aimed at dissecting whether T_{regs} expressing different *FOXP3* variants could have a dominant role in BC immune evasion (Fig. 1A). We analyzed the frequency of FOXP3$^+$ (all FOXP3 transcript variants) and FOXP3E2$^+$ T_{regs} (FOXP3 variants retaining Exon2) in the PB and tumor-infiltrating lymphocytes (TILs) from two different cohorts of patients with newly diagnosed, untreated ER$^+$PR$^+$[hormone receptor–positive (HR$^+$)]–HER2$^-$ breast cancer (BC) and nonmalignant breast fibroadenoma (BF) (table S1). Freshly resected breast tissue was mechanically dissociated into a single-cell homogenate to enrich TILs (*39*). Flow cytometric analysis revealed a dominance of CD4$^+$ T cells in BC, also confirmed by a lower CD8$^+$/CD4$^+$ ratio compared to that in BF tissue (0.86 versus 2.51) (Fig. 1B). In addition, BC tissue shows a more abundant infiltrate of FOXP3$^+$ T_{regs} as compared to BF tissue, and a higher frequency of T_{regs} is detected within the tissues as compared to PB from both patients with BC and BF (Fig. 1C). We detected a significant enrichment of FOXP3E2$^+$ T_{regs} in BC tissue (i.e., TIL-FOXP3E2$^+$) compared to that in BF and PB (both from patients with BC and BF) (Fig. 1D). To estimate the relative frequency of FOXP3E2$^+$ compared to the overall T_{reg} compartment, we measured the FOXP3E2$^+$/FOXP3$^+$ ratio (E2 ratio) and found that FOXP3E2$^+$ T_{regs} were more abundant both in the TME and PB of patients with BC compared to those of patients with BF (Fig. 1E). Furthermore, we compared the percentage and ratio of FOXP3E2$^+$ and FOXP3$^+$ T_{regs} in the TIL and PB of our BC cohort. The percentage of TIL-FOXP3E2$^+$ T_{regs} was, on average, 8.33%, and the TIL-FOXP3$^+$ represented 14.75% (fig. S1A). The percentage of PB-derived FOXP3E2$^+$ T_{regs} (PB-FOXP3E2$^+$) and PB-FOXP3$^+$ were, instead, 2.57 and 5.27% of the total CD4$^+$ T cells, respectively (fig. S1A). Notably, the ratio between FOXP3E2$^+$ and total T_{regs} in patients with BC was significantly higher in TIL compartment as compared to that in PB lymphocytes, suggesting that FOXP3E2$^+$ T_{regs} preferentially accumulate in the TME (mean E2 ratio is equal to 0.64 in TIL and 0.54 in PB) (Fig. 1E and fig. S1B). Notably, the CD8$^+$/T_{reg} ratio was significantly lower in BC (both in PB and TIL) and inversely correlated with the percentage of TIL-FOXP3E2$^+$ in the TME [correlation coefficient (r) = −0.603, P = 0.001] (Fig. 1, F and G), while no correlation was observed with the TIL-FOXP3$^+$ (not shown). As the CD8$^+$/T_{reg} ratio is considered a reliable marker of antitumor-specific T cell response (*34*), our data suggest that the FOXP3E2$^+$ T_{reg} subset mainly accounts for the suppression of the immune response to cancer. Immunohistochemical (IHC) staining and digital quantitative image analysis confirmed the higher infiltration of FOXP3$^+$ and FOXP3E2$^+$ T_{regs} in BC tissue compared to that in BF (Fig. 1, H to O). Our results unveil a distinct prevalence of FOXP3E2$^+$ T_{regs} in human BC that is not observed in nonmalignant forms of breast tumors (i.e., BF) and inversely correlates with antitumor immune response.

FOXP3E2 transcript levels in BC tissue mark an immune landscape that correlates with reduced overall survival

To determine whether the increased percentage of FOXP3E2$^+$ T_{regs} is associated with BC prognosis in general, we examined RNA sequencing (RNA-seq) data from about 1000 participants (990 BC tissues and 112 tumor-adjacent normal tissues) in the TCGA (The Cancer Genome Atlas) Splicing Variant Database (TSVdb) that includes information on alternative splicing (*40*). We found that primary BCs (69.2% HR$^+$HER2$^-$, 12.6% HR$^+$HER2$^+$, and 18.2% HR$^-$HER2$^-$) expressed higher levels of FOXP3 transcripts compared to normal breast tissue (NT) (64.00 versus 13.40) (Fig. 2A). However, FOXP3 transcript levels did not correlate with patient overall survival when patients with BC were stratified either on their median value (Q2) or on their upper quartile range (Q3) (Fig. 2, B and C, and fig. S1, C and D). Thus, we measured the expression of the five different FOXP3 isoforms [schematically represented in fig. S1E and reported in the University of California Santa Cruz (UCSC) bank; (*33*)], and we found that four of them were up-regulated in BC tissue compared to that in NT (fig. S2, A to D), but none correlated with overall survival (fig. S2, E to L). Then, we estimated the ratio of FOXP3 Exon2–containing transcripts relative to the other variants, and patients with BC were stratified into low (<Q3 = 0.09)– and high (>Q3 = 0.29)–E2 ratio groups (Fig. 2, D and E). This analysis clearly shows that the difference in FOXP3E2 expression between the two groups was inversely correlated with patient overall survival (log-rank P = 0.01, $\chi 2$ = 6.2) (Fig. 2, F and G). No difference in total FOXP3 expression between the two groups was observed (fig. S3A); also, we did not find correlation when patients with BC were stratified on the median value of the E2 ratio (fig. S3, B to D). Notably, TCGA also included HER2$^+$ as well as the most aggressive triple-negative tumors, thus suggesting a general association between the enrichment of FOXP3E2$^+$ T_{regs} within the tumor and BC prognosis.

To gain insights into the nature of the local TME (*41*, *42*), we characterized gene expression patterns of high– and low–FOXP3E2$^+$/FOXP3$^+$ (E2) ratio BC groups. Analysis of differentially expressed genes (DEGs) identified 702 DEGs (523 down-regulated and 179 up-regulated genes) (Fig. 2H). Gene Ontology (GO) revealed a significant enrichment of genes belonging to immunoregulatory pathways in the BC group showing high E2 ratio. These immunoregulatory genes included humoral immune response, complement activation, and antigen receptor–mediated signaling (Fig. 2I). Among all, the up-regulation of *BTN1A1*, *FCRL1*, *CXCR5*, *AIRE*, and *ZAP70* was

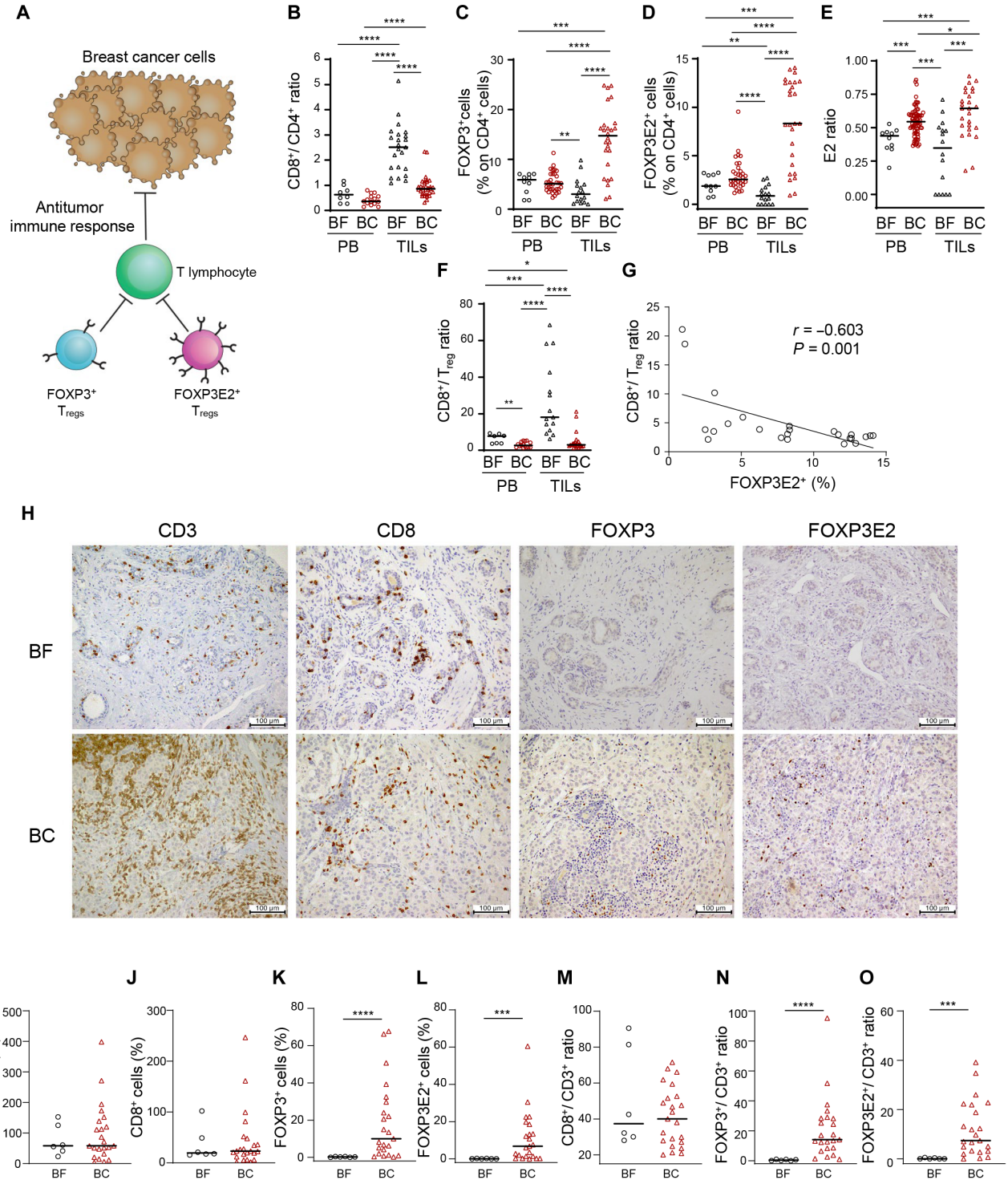

Fig. 1. Characterization of the immune infiltrate in PB and primary tissue from patients with BC and BF. (**A**) Schematic representation of FOXP3$^+$ and FOXP3E2$^+$ T_{regs} in tumor immune escape. (**B**) CD8$^+$/CD4$^+$ ratio, % of (**C**) FOXP3$^+$ and (**D**) FOXP3E2$^+$ cells (gated on CD4$^+$), (**E**) FOXP3E2$^+$/FOXP3$^+$ ratio (E2 ratio), and (**F**) CD8$^+$/T_{reg} ratio in peripheral blood (PB; dots) and tumor-infiltrating lymphocytes (TILs; triangles) from patients with BF (white empty) and BC (red empty). In (B) to (F), represented data are for BF at least $n = 7$ and $n = 15$ and for BC at least $n = 15$ and $n = 24$ (respectively, for TILs and PB). (**G**) Correlation between % of FOXP3E2$^+$ and CD8$^+$/T_{reg} ratio in TILs from patients with BC ($n = 24$). (**H**) Representative immunohistochemical (IHC) staining of primary BC and BF tissue showing CD3$^+$, CD8$^+$, FOXP3$^+$, and FOXP3E2$^+$ cells. Immunohistochemistry-based quantification of (**I**) % of CD3$^+$, (**J**) CD8$^+$, (**K**) FOXP3$^+$, (**L**) FOXP3E2$^+$ cells, (**M**) CD8$^+$/CD3$^+$ ratio, (**N**) FOXP3$^+$/CD3$^+$ ratio, and (**O**) FOXP3E2$^+$/CD3$^+$ ratio [respectively, white dots ($n = 6$) for BF and red triangles ($n = 23$) for patients with BC]. Data are presented as median values. Each data point represents a different individual (i.e., independent biological samples) [(G) and (I) to (O)] or experimental replicates [(B) to (F)]. Statistical analyses were performed by using Mann-Whitney *U* test (two tails) [(B) to (F) and (I) to (O)] and Spearman *r* correlation test (G). *$P \leq 0.05$; **$P \leq 0.01$; ***$P \leq 0.005$; ****$P \leq 0.0001$.

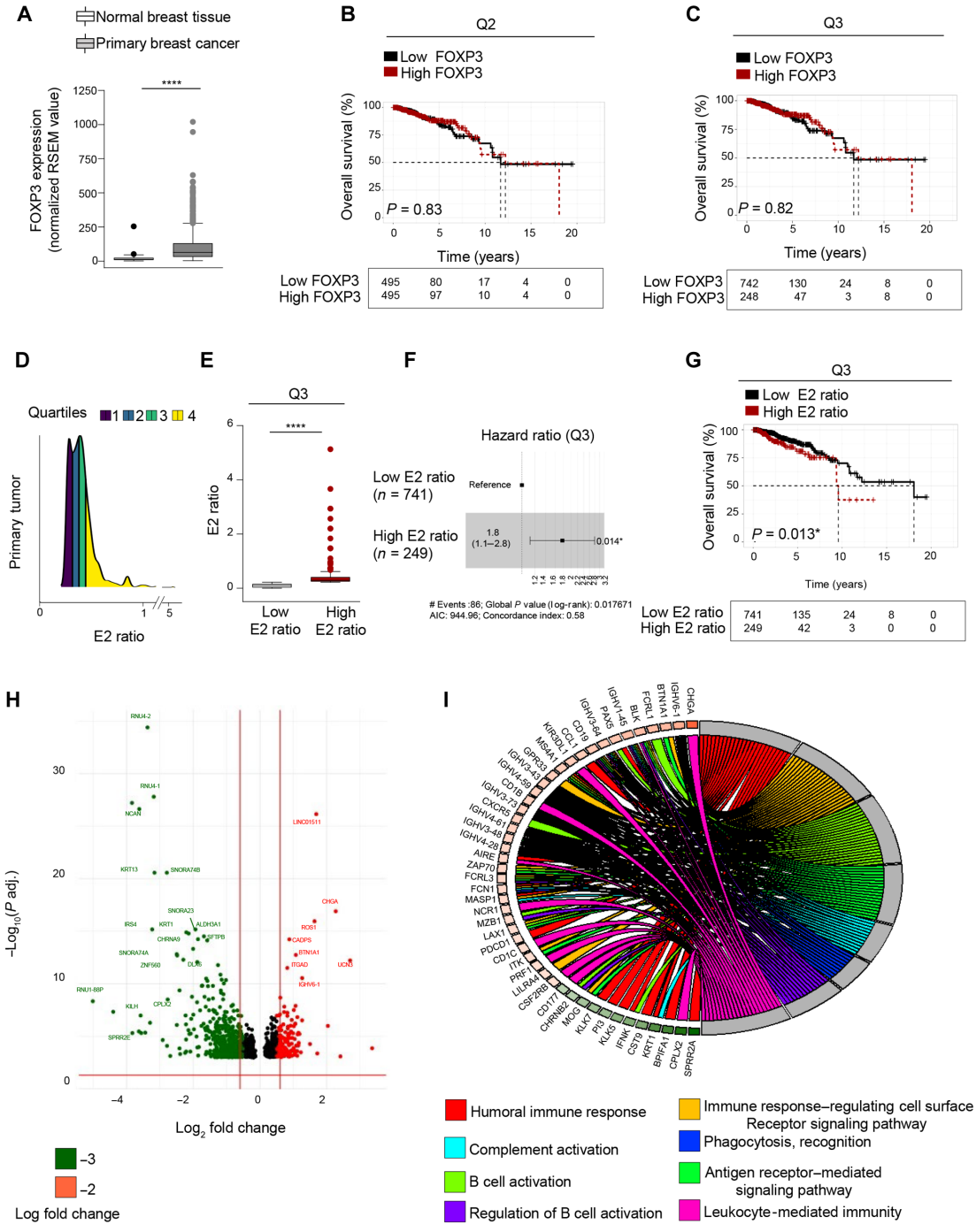

Fig. 2. FOXP3E2 transcript analysis from primary BC tissues delineates a subgroup of patients with poor prognosis and a distinctive gene expression profile. (**A**) FOXP3 transcripts in normal ($n = 112$) and primary BC ($n = 990$) tissues. Data represent normalized RNA-seq by expectation maximization (RSEM) value obtained by RNA-seq analysis of datasets in the TCGA database. (**B** and **C**) Kaplan-Meier survival curve of patients with BC stratified into low– and high–FOXP3 expression levels within the primary tumor based on its Q2 ($n = 495$ and 495) or Q3 ($n = 742$ and 248) value. (**D**) Interquartile distribution of the FOXP3E2/FOXP3 ratio calculated in the primary BC tissue ($n = 990$). (**E**) Patients with BC were stratified into low ($n = 741$) and high ($n = 249$) FOXP3E2/FOXP3 ratio (E2 ratio) according to the Q3 value cutoff. (**F**) Hazard ratio (= 1.8, confidence interval of 1.1 to 2.8, Cox $P = 0.014$) and (**G**) Kaplan-Meier survival curve of patients with BC with low ($n = 741$) and high ($n = 249$) E2 ratios according to Q3 value cutoff. AIC, Akaike's Information Criterion. (**H**) Volcano plot of differentially expressed genes (DEGs) obtained by applying a threshold of $\log_2$ fold change > ±0.05 (x axis) and a P adj. < 0.001 (y axis) in the two groups of patients with BC. Dots represented single genes: 179 up-regulated (red) and 523 down-regulated (green) in the high-ratio BC group. (**I**) Circular composition overview plot for selected Gene Ontology (GO) pathways (represented in different colors) overrepresented among DEGs in high– versus low–FOXP3E2/FOXP3 ratio BC groups. GO analysis was performed by DAVID database. Gene color scale indicates the relevant fold change values (red, up-regulated; and green, down-regulated). Data are presented as median values [(A) and (E)]. Statistical analyses were performed by using Mann-Whitney U test (two tails) [(A) and (E)], Multivariate Cox regression model reference [(B), (C), and (G)] and log-rank test (F). ****$P \leq 0.0001$.

noteworthy (Fig. 2I), indicating a dominant immunological signature (*43*, *44*). Consistently, gene set enrichment analysis (GSEA)–Kyoto Encyclopedia of Genes and Genomes analysis showed five sub-gene sets activated in the high–E2 ratio BC group [chemokine signaling, hematopoietic cell lineage, glycerolipid metabolism, cyclic adenosine 3′,5′-monophosphate signaling, and neuroactive ligand-receptor interaction; (*45*)] (fig. S4A). Up-regulation of *WNT3a*, *ESRG*, *NANOGP1*, and *NEFL*, instead, suggested the acquisition of stem cell–like features (fig. S4B) (*46*–*49*). Overall, these analyses reveal that FOXP3E2 marks a distinctive group of patients with BC characterized by worst clinical outcomes (i.e., lower survival) and likely associated with increased immunoregulation and stemness.

Breast tumors with a high FOXP3E2 ratio show greater clonal selection

To better understand the relationship between high E2 ratio and poor BC clinical outcome, we investigated mutations in cancer driver genes. To this aim, we first characterized genome variants in the high– and low–E2 ratio BC groups. We observed comparable tumor mutational burden in the two groups (fig. S5, A and B), with *PIK3CA* and *TP53* mutations dominating the landscape (fig. S5, C to F) consistently with previous reports (*50*). Other genes, however, harbored coding mutations in at least 6% of the samples: *CDH1*, *MAP3K1*, *KMT2C*, *GATA3*, RYR2, and *FLG* (fig. S5, C to F). Well-known germline mutations in *BRCA1* and *BRCA2* were identified in less than 5% of patients with BC of both groups (fig. S6). We then examined pairwise associations between somatic events to explore co-mutations and found mutual exclusivity between *TP53*, *PIK3CA*, and *CDH1* mutations in patients with BC of both groups (Fig. 3, A and B). The phosphatidylinositol 3-kinase (PI3K)/Akt mutation marked specifically the high–FOXP3E2 ratio BC group [false discovery rate (FDR) < 0.05] (Fig. 3, A and B), further suggesting increased cancer stem-like features and cell survival (*51*, *52*). Furthermore, we detected a lower frequency of co-mutations in the high–FOXP3E2 ratio BC group despite the comparable tumor mutational burden (Fig. 3, A to D, and fig S5, A and B). Last, we used the normalized ratio of nonsynonymous to synonymous somatic mutations (dN/dS ratio) across all variants (as well as on a per gene basis) to distinguish genes and specific mutations under purifying, neutral, and positive selection (*53*). We observed three common driver genes in both groups of patients (i.e., TP53, PI3K, and CDH1), while KMT2C and PTEN were found only in the low–FOXP3E2 ratio BC group (Fig. 3, C and D). In-depth analysis of these driver genes shows a mutual exclusivity only in the high–FOXP3E2 ratio BC group (Fig. 3, C and D). In addition, clonal evolutional analysis revealed a lower frequency of allelic variants in the high–FOXP3E2 ratio BC group (Fig. 3E). Overall, this suggests a stronger selection of tumors with a high FOXP3E2 ratio possibly related to immunoediting (*4*, *54*).

BC tumors with a high FOXP3E2 ratio show mutational signatures associated with dMMR and a dominant immune landscape

The sub-clonal nature of the high–E2 ratio BC group suggests a tumor evolution and selection (*55*, *56*), which implies different molecular mechanisms including spontaneous and enzymatic deamination of the cytosine base (*57*, *58*). To gain insights into the dynamics of the mutational signature that shapes both BC groups, we interrogated COSMIC mutational signatures that have been associated with specific pathways (*30*). Signatures associated with spontaneous deamination of 5-methylcytosine and APOBEC cytidine deaminase were detected in both the high– and low–E2 ratio BC groups (fig. S7, A and B). Enrichment analysis of APOBEC motif, characterized by C-to-T transitions and C-to-G transversions in tCw motifs (W = A or T), in the high– and low–FOXP3E2 ratio BC groups showed a similar prevalence of tCw mutations (34% APOBEC versus 9% non-APOBEC in the low–E2 ratio BC group and 38% APOBEC versus 9% non-APOBEC in the high–E2 ratio BC group) (fig. S7, C and D), with no change in the global DNA methylation (fig. S7E). Defects in polymerase POLE, which occur in ultra-hypermutators, have instead been observed only in the low–E2 ratio BC group (Fig. 4A); however, we did not find difference in tumor mutational burden (fig. S5, A and B) and number of neoantigens (fig. S7F). Notably, the signature associated with defective DNA mismatch repair (dMMR) was specific for the high–E2 ratio BC group (Fig. 4B). MMR is a fundamental DNA repair pathway essential to maintain genome stability during cellular replication (*59*), and defects have been considered driver of endocrine treatment resistance in 15 to 17% of patients with $ER^+/HER2^-$ BC (*60*, *61*). To better dissect this pathway, we evaluated gene and protein expression of MMR-associated factors. We did not observe changes in MMR gene expression (e.g., *MLH1*, *MLH3*, *MSH2*, *MSH3*, *MSH6*, and *PMS2*) (fig. S8A). However, analysis of reverse-phase protein array (RPPA) showed, instead, high levels of ATM, ATM_pS1981, UVRAG, and XPA and low levels of BRCA2, CHK2, DDR1, DDR1_pY513, DNA PolG, MSH2, MSH6, Wee1, X53BP1, and DNMT1 in patients with BC with a high FOXP3E2 ratio (Fig. 4C), suggesting that DNA damage response (DDR) might be specifically dysregulated in these patients with cancer. Notably, patients with BC with a high FOXP3E2 ratio also showed higher expression of immune-related signatures as compared with the low–E2 ratio group (i.e., CD20, CD38, CD4, CD45, IL6, JAG1, and ZAP70) (Fig. 4D). This increase in immune pathways was also confirmed by enrichment analysis of the differentially expressed probes using Metascape (Fig. 4D) (*62*). Notably, immune cell deconvolution shows only a slight increase in the number of endothelial cells between the two subgroups with no difference in the immune cell compartments (fig. S8B). Together, our analyses unveil that FOXP3E2 marks a subgroup of breast tumors characterized by defective DNA damage repair and a dominant immunomodulatory signature.

Increased IC expression and stronger suppressive capability is associated with FOXP3E2 expression in T_{regs} of HR^+ BC

As both our ex vivo analyses of patients with HR^+ BC and TCGA data mining suggest an association between $FOXP3E2^+$ T_{regs} and immune modulation in the TME, we evaluated their immunosuppressive function. To this aim, we initially checked the expression of a range of co-inhibitory molecules, known to modulate tumor immune responses and up-regulated in tumor-infiltrating T_{regs} (*15*, *21*, *22*, *63*) (e.g., ICs, such as CTLA-4, PD-1, and TIGIT), in TIL- and PB-derived $CD4^+$ T cells from patients with BC (Fig. 5 and fig. S9). We found that TIL-$FOXP3E2^+$ T_{regs} have increased percentage of Helios and CCR8 and higher levels of Helios and CTLA-4 than TIL-$FOXP3^+$ T_{regs}. Moreover, when compared to PB, TIL-$FOXP3E2^+$ T_{regs} show increased expression of Helios, inducible costimulator (ICOS), CTLA-4, PD-1, TIGIT, and CCR8 and higher proliferative capacity, as pointed out by $Ki67^+$ frequency (Fig. 5 and fig. S9). Co-expression

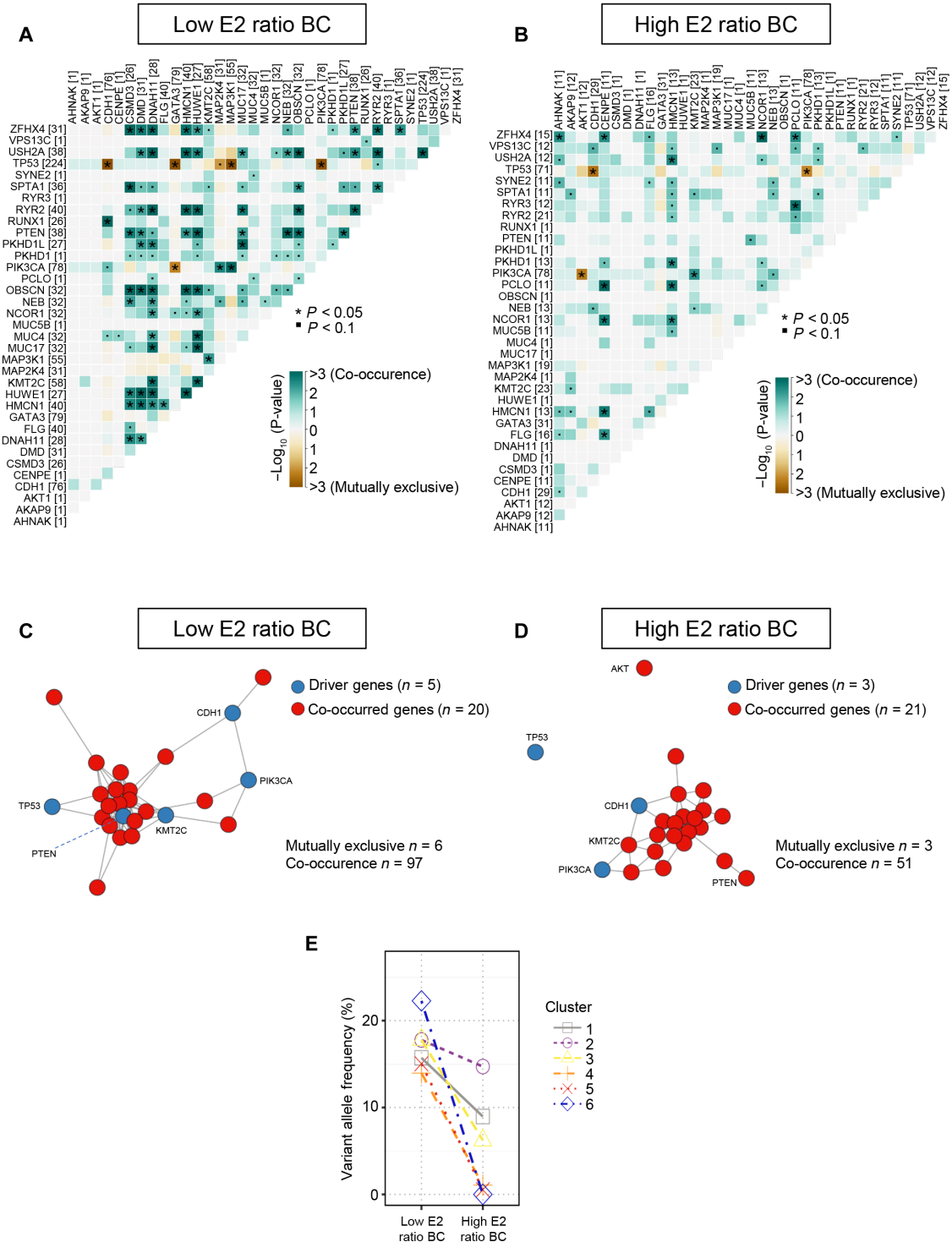

Fig. 3. Reduced co-mutation frequency and co-occurrence characterizes the BC group with a high FOXP3E2/FOXP3 ratio. (**A** and **B**) Somatic interaction analysis between gene pairs showing that co-occurring mutations (green squares) and mutually exclusive mutations (brown squares) were detected using somaticInteractions function of Maftools (v.2.12.0), which performs pair-wise Fisher's exact tests to detect significant [Benjamini-Hochberg false discovery rate (FDR) < 0.1] pairs of genes. The intensity of the color is proportionate to the $-\log_{10}$ (*P* value). (**C** and **D**) Diagram reporting the cancer network of patients with BC separated into low and high FOXP3E2/FOXP3 ratios, including nodes (driver genes) and edges (co-occurrences), obtained by WES analysis from TCGA. Red circles represent driver genes, and blue circles represent all occurrences found. The solid black links represent the key links found by the co-occurrence analysis. Genes were considered to have evidence of positive selection (driver gene) if the reported dN/dS ratio qglobal_cv was <0.05 for missense mutations, truncating variants, all substitutions, or indels. (**E**) Variant allele frequency (%) showing the mean of variant clusters across groups. ClonEvol was used to infer consensus clonal evolution models using the variant clusters generated by the Maftools R package. Statistical analyses were performed by using by Benjamini-Hochberg multiple testing correction.

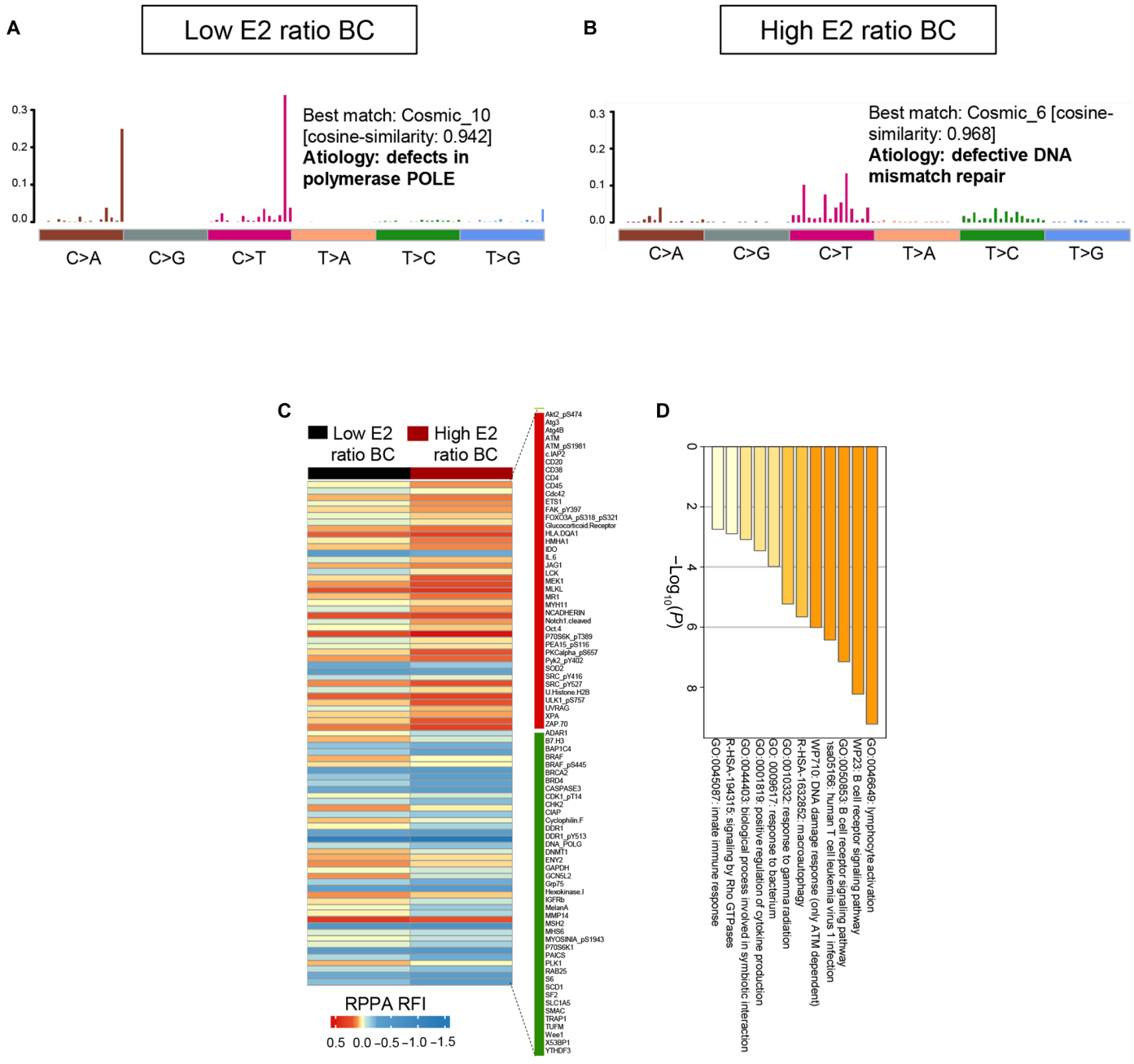

Fig. 4. dMMR and specific mutational signatures in patients with BC with a high FOXP3E2/FOXP3 ratio. (**A** and **B**) Mutational signatures identified in patients with BC with low and high FOXP3E2/FOXP3 ratios, respectively. The *y* axis indicates exposure of 96 trinucleotide motifs to overall signature. In each plot, we report the best match against validated COSMIC signatures (COSMIC v.2) and cosine similarity value alongside the proposed etiology. (**C**) Supervised hierarchical clustering analysis of TCGA-BC reverse-phase protein array (RPPA) results using an analysis of variance (ANOVA) FDR *P*-value threshold lower than 0.05. On the basis of this threshold, 81 probes were differentially altered in the high–E2 ratio group, with 40 probes up-regulated (red bar) and 41 down-regulated (green bar). (**D**) Enrichment analysis of the differently expressed probes using Metascape. Statistical analyses were performed by using Cophenetic correlation. GTPases, guanosine triphosphatases.

of CTLA-4 and PD-1 or TIGIT and CCR8 was higher in TIL-FOXP3E2$^+$ than that in PB-FOXP3E2$^+$ T_{regs} (Fig. 5), thus suggesting that this T_{reg} subpopulation exerts a dominant role in cancer evasion/immunosuppression. This is particularly relevant as elevated CCR8 expression in TIL-T_{regs} is related to poor prognosis in several cancer types (*19*, *64*). Moreover, the increased expression of Helios and ICOS revealed that FOXP3E2$^+$ T_{regs} infiltrating the tumor had a hyper-activated phenotype. In addition, the evidence that pS6 levels, reflecting mammalian target of rapamycin (mTOR) kinase activity, were reduced specifically in TIL-FOXP3E2$^+$ compared to that in the PB counterpart suggests a detrimental role for the mTOR pathway in the suppression of antitumor response.

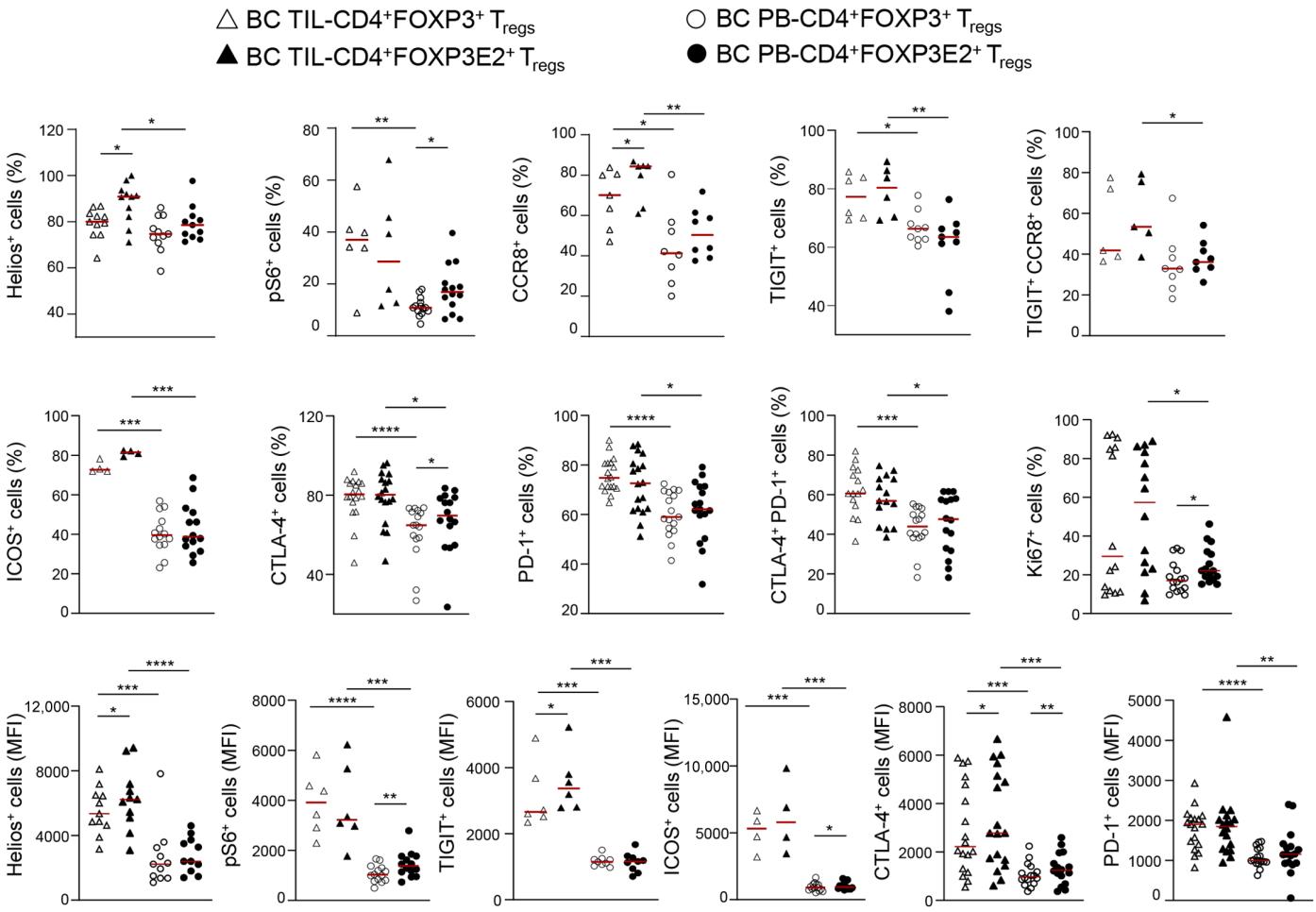

Fig. 5. Highly immunosuppressive FOXP3E2$^+$ T_{regs} preferentially accumulate in TILs of patients with newly diagnosed HR$^+$ BC. Cumulative data of flow cytometry analysis showing cell percentage and mean fluorescence intensity (MFI) of Helios$^+$, pS6$^+$, CCR8$^+$, TIGIT$^+$, ICOS$^+$, CTLA-4$^+$, PD-1$^+$, and Ki67$^+$ cells (gated on CD4$^+$FOXP3$^+$ and CD4$^+$FOXP3E2$^+$) in freshly isolated TILs (at least $n = 4$, BC TIL) and PB (at least $n = 9$, BC PB) from patients with BC. Data are presented as median values. Statistical analysis was performed by using Wilcoxon and Mann-Whitney *U* test (two tails); *$P \leq 0.05$; **$P \leq 0.01$; ***$P \leq 0.005$; ****$P \leq 0.0001$.

Overall, the increased expression of Helios and IC in the FOXP3E2$^+$ T_{regs} proposes that they might have a higher immunosuppressive capacity in cancer.

We tested this hypothesis through an in vitro carboxyfluorescein diacetate succinimidyl ester (CFSE)–based suppression assay by culturing blood-derived conventional T cells (T_{convs}) with autologous T_{regs} from patients with BC. T_{regs} from patients with BC show stronger suppressive capacity compared to T_{regs} from age-matched female healthy donors (HDs) (Fig. 6A). When compared to HDs, patients with BC displayed increased E2 PB ratio (0.54 versus 0.49) (Fig. 6B) and higher frequency of TIGIT$^+$, CCR8$^+$, TIGIT/CCR8, and CTLA-4/PD-1 double-positive PB-FOXP3E2$^+$ T_{regs} (Fig. 6C and fig. S10A). As ICOS levels were higher in TIL-FOXP3E2$^+$ T_{regs} compared to that in the PB, this suggested a preferential recruitment of ICOS$^+$FOXP3E2$^+$ T_{regs} in the TME (Figs. 5 and 6C). Notably, the median of the E2 PB ratio within the BC cohort (Q2 = 0.545) represents a "hub value" almost coincident with that corresponding to the Q3 value of HDs (Q3 = 0.546) (Fig. 6D), suggesting that E2 PB ratio might as well be associated with stronger immune suppression.

Breast tumor–derived supernatants promote FOXP3E2$^+$ iT$_{reg}$ generation through the CXCL12/CXCR4 axis

FOXP3$^+$ T_{regs} support tumor tolerance (*1*), but how their generation and recruitment are regulated in the TME remains largely unknown. To understand whether T_{reg} generation could be greater in patients with BC, we stimulated freshly isolated T_{convs} from HDs and patients with HR$^+$ BC via T cell receptor (TCR) to measure the expression of FOXP3 during the in vitro generation of inducible T_{regs} (iT$_{regs}$) (*35*). Western blot analyses showed that both FOXP3 and FOXP3E2 isoforms were significantly greater in BC compared to those in HDs at 24 hours (Fig. 7, A to C). To explore the contribution of the TME, we added 30% of supernatants derived from human NT and BC cell lines (i.e., MCF10 and MCF7, respectively) to the culture medium of HD-derived T_{convs} during their differentiation into iT$_{regs}$. We found that the addition of supernatants from the BC cell line MCF7 selectively promoted the induction of FOXP3E2 in iT$_{regs}$ measured at 24 hours by fluorescence-activated cell sorting (FACS) analysis (fig. S10, B and C). Because MCF7 cell lines represent a reductive model of study, we directly assessed the contribution of the intratumoral milieu from breast tumor biopsies in iT$_{reg}$

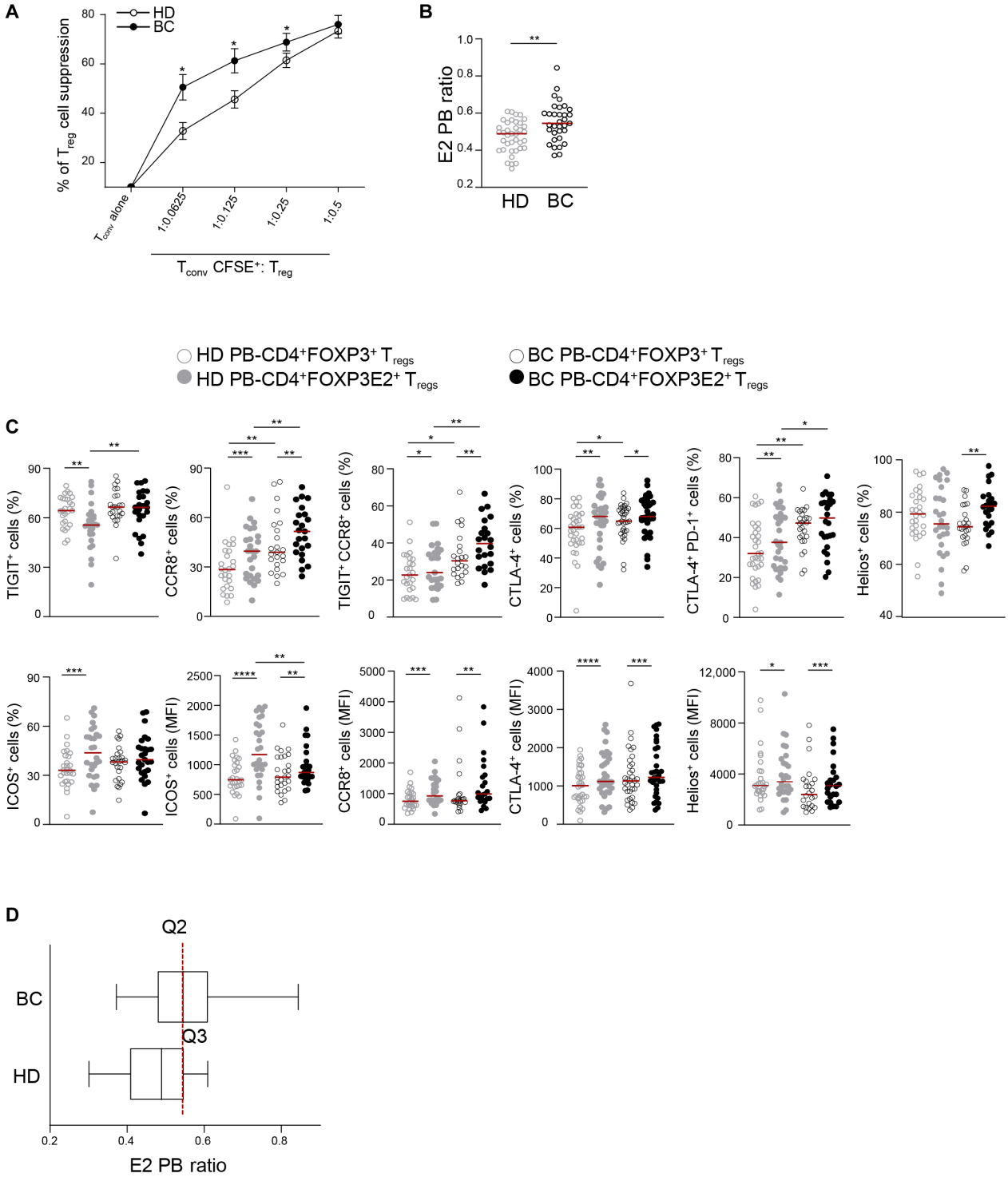

Fig. 6. Higher IC expression in T_{regs} from patients with HR^+ BC correlates with increased $FOXP3E2^+/FOXP3^+$ ratio and peripheral T_{reg} suppressive function. (**A**) Percentage of suppression of T_{regs} in coculture with carboxyfluorescein diacetate succinimidyl ester (CFSE)–labeled T_{convs} at different proportions of T_{regs}/T_{convs}, purified from HDs ($n = 20$) and patients with BC ($n = 16$). (**B**) FOXP3E2 PB ratio (E2 PB ratio) calculated by flow cytometry quantification of the ratio of $CD4^+FOXP3E2^+/CD4^+FOXP3^+$ T_{regs} from PB of HDs ($n = 38$) and patients with BC ($n = 33$). (**C**) Percentage of $TIGIT^+$, $CCR8^+$, $TIGIT^+/CCR8^+$, $CTLA\text{-}4^+$, $CTLA\text{-}4^+/PD\text{-}1^+$, $Helios^+$, and $ICOS^+$ T_{regs} and MFI of ICOS, CCR8, CTLA-4, and Helios on $CD4^+FOXP3^+$ and $CD4^+FOXP3E2^+$ T_{regs} from PB of HDs (at least $n = 25$) and patients with BC (at least $n = 22$). (**D**) Box plot representation of the E2 PB ratio (median, minimum to maximum values, and quartiles) from patients with BC ($n = 33$) and HDs ($n = 38$). Each symbol shows independent biological samples [(B) to (D)] or experimental replicates (A). Data are presented as median values. Statistical analysis was performed by using Wilcoxon and Mann-Whitney *U* test (two tails); $*P \leq 0.05$; $**P \leq 0.01$; $***P \leq 0.005$; $****P \leq 0.0001$.

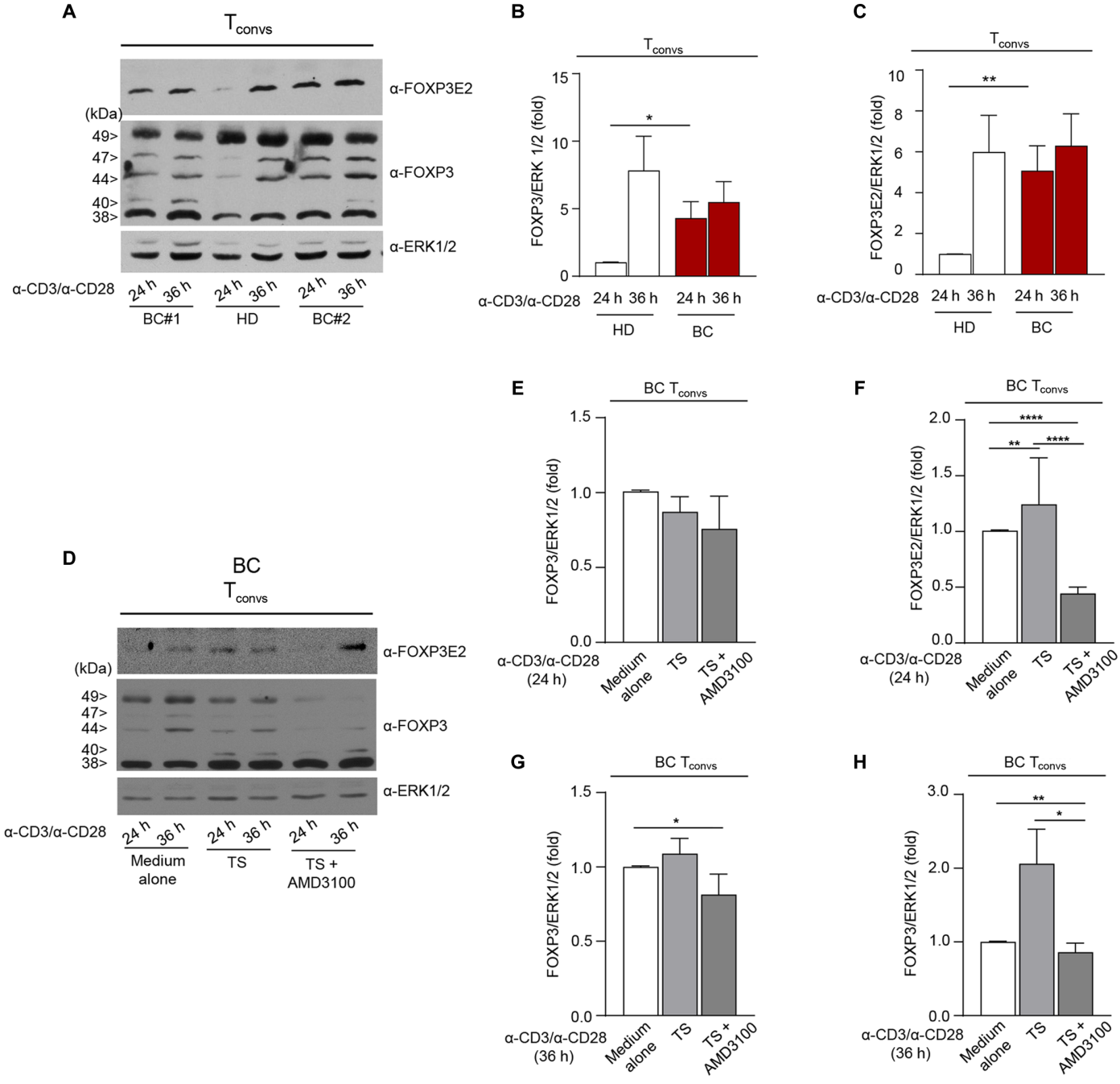

Fig. 7. Breast TS–derived CXCL12 induces FOXP3E2 in iT_{regs} of HR^+ BC. (**A**) Representative immunoblot and (**B** and **C**) densitometry of FOXP3 (all splicing variants) and FOXP3E2 in T_{convs} from HD (white columns) and BC (red columns) stimulated in vitro for 24 and 36 hours (h) with anti-CD3/anti-CD28 mAbs (0.1 bead per cell) to obtain inducible T_{regs} (iT_{regs}). FOXP3 and FOXP3E2 were normalized to total extracellular signal–regulated kinase 1/2 (ERK 1/2) and presented relative to results obtained for 24-hour TCR-stimulated HD-T_{convs}. Data were from $n = 3$ independent experiments from four HDs and six patients with HR^+ BC [(B) and (C)]. (**D**) Representative immunoblot and (**E** to **H**) densitometry of FOXP3 (all splicing variants) and FOXP3E2 in T_{convs} from patients with BC after 24 [(E) and (F)] and 36 [(G) and (H)] hours of in vitro TCR stimulation, in the presence of 5% of TS, alone or in combination with AMD3100 (50 μM). FOXP3 and FOXP3E2 were normalized to total ERK 1/2 and presented relative to results obtained for 24 [(E) and (F)]– and 36 [(G) and (H)]–hour TCR-stimulated BC-T_{convs} (in medium alone). Data were from $n = 5$ independent experiments from at least four patients with BC, presented as means ± SEM. Statistical analyses were performed by using the Mann-Whitney *U* test (two tails). $^*P \leq 0.05$; $^{**}P \leq 0.01$; $^{****}P \leq 0.0001$. h, hours.

generation. To this, we performed an unbiased measurement of cytokines/chemokines/growth factors of tumor supernatants (TSs) derived from freshly resected HR^+ breast tumor biopsies by multiplex enzyme-linked immunosorbent assay system. Among all, we detected a large amount of CXCL12/SDF1 (Table 1), a cancer-associated fibroblast (CAF)–derived chemokine known to trigger the accumulation of T_{regs} in the TME (*1*). To understand the functional role of CXCL12 in T_{reg} induction, we added 5% of TSs derived from breast tumor biopsies of patients with HR^+ BC to the culture medium of autologous T_{convs} to follow their in vitro conversion into iT_{regs}, with or without CXCL12 antagonist (AMD3100) (*65*–*67*). Data derived from Western blot analyses showed that TS supplementation selectively fostered the expression of FOXP3E2 splicing variants and CXCL12/SDF1 likely mediated this effect as the induction was not observed in the presence of its antagonist (Fig. 7, D to H). This is in agreement with recent findings, suggesting that T_{regs} in human BC derive from antigen-experienced T_{convs} converting into secondary iT_{regs} via intratumoral activation (*68*). These data pinpoint CXCL12 as a key factor enforcing the generation of highly immunosuppressive FOXP3E2$^+$ T_{regs} in HR^+ BC and provide evidence for the contribution of the TME in tumor tolerance.

Table 1. Chemokine and cytokine levels in TSs derived from freshly resected BC biopsy. Supernatants derived from at least five freshly resected BC biopsies of patients with BC were tested using the human Bio-Plex multiplex chemokines assay kit (see Materials and Methods for details). Data were presented as median [interquartile range (IQR)]. nd, not detectable.

Chemokine/cytokine	pg/ml (median [IQR])
IL-1β	0.135 [0.052–0.222]
IL-2	nd
IL-4	1.150 [0.850–2.060]
IL-6	1.110 [0.785–3.285]
IL-8/CXCL8	1.980 [1.120–2.953]
IL-10	0.495 [0.400–0.792]
IL-16	233.3 [115.2–727.9]
GM-CSF	2.120 [1.440–2.665]
IFN-γ	0.560 [0.370–0.990]
IP-10/CXCL10	4.510 [0.945–91.72]
MIP-1α	16.58 [7.045–26.22]
TNF-α	2.595 [1.705–5.230]
I-309/CCL1	36.66 [4.900–68.42]
MCP-1/CCL2	16.97 [7.435–26.61]
MCP-2/CCL8	0.430 [0.230–0.945]
MCP-3/CCL7	nd
MCP-4/CCL13	1.830 [0.940–3.755]
MIP-1δ/CCL15	14.27 [6.170–16.87]
MIP-3β/CCL19	30.13 [26.28–43.63]
MIP-3α/CCL20	nd
TARC/CCL17	nd
6Ckine/CCL21	11824 [895.7–16544]
MDC/CCL22	11.11 [6.870–19.05]
MPIF1/CCL23	9.340 [1.853–11.71]
TECK/CCL25	106.3 [64.15–146.3]
Eotaxin	7.750 [5.973–9.300]
Eotaxin-2/CCL24	6.965 [4.213–11.63]
Eotaxin-3/CCL26	4.140 [2.390–8.370]
CTACK/CCL27	4.640 [0.665–9.145]
MIF	34403 [17526–41803]
Fractalkine/CX3CL1	14.97 [9.703–26.98]
Gro-α/CXCL1	29.84 [25.26–50.68]
Gro-β/CXCL2	3.340 [2.204–37.55]
ENA-78/CXCL5	nd
GCP-2/CXCL6	1.660 [1.325–45.97]
MIG/CXCL9	4.985 [1.178–170.4]
I-TAC/CXCL11	0.390 [0.120–0.760]
SDF-1α$^+$β/CXCL12	80.67 [58.85–132.0]
BCA1/CXCL13	1.410 [0.160–16.66]
SCYB16/CXCL16	29.96 [18.72–76.13]

Blood-derived FOXP3E2 ratio reflects poor prognosis in patients with HR^+ BC, and tumor-derived FOXP3E2 predicts survival also in other human cancers

We observed that T_{reg} peripheral suppression in patients with BC directly correlated with the FOXP3E2 (E2) TIL ratio ($r = 0.66$, $P = 0.021$) (Fig. 8A). Specifically, patients with BC with a high E2 TIL ratio (≥0.64) showed higher peripheral T_{reg} suppression than the ones with a low ratio (<0.64) (Fig. 8B). The more TIL-FOXP3E2$^+$ T_{regs} they had, the greater the peripheral suppressive capacity. We observed that the E2 PB ratio strictly mirrored the E2 TIL ratio, as patients with BC with a high E2 TIL ratio also exhibited higher E2 PB ratio (Fig. 8C). Consistently, T_{regs} from patients with BC with a higher E2 PB ratio showed increased suppressive activity compared to the low–E2 PB ratio group (Fig. 8D). Furthermore, FOXP3E2$^+$ T_{regs} from the high–E2 PB ratio BC group displayed an immune phenotype distinct from the FOXP3$^+$ T_{regs}, with enhanced expression of Helios, ICOS, CTLA-4, and CCR8 and co-expression of CTLA-4/PD-1 and TIGIT/CCR8 (Fig. 8E and fig. S11A), thus mirroring the hyperactivated phenotype observed in TIL-FOXP3E2$^+$ T_{regs} (Fig. 5). Notably, FOXP3E2$^+$ T_{regs} from the high–E2 PB ratio group expressed low pS6 levels compared to FOXP3E2$^+$ T_{regs} from the low–E2 PB ratio group (Fig. 8E), according to what previously observed in TIL-FOXP3E2$^+$ versus TIL-FOXP3$^+$ (Fig. 5). This could further support that mTOR activity perturbs the suppression of antitumor-specific immune response. Overall, our data indicate that the E2 ratio in the PB reflects the infiltration of highly immunosuppressive FOXP3E2$^+$ T_{regs} in the TME.

As our findings uncovered a direct connection between peripheral- and tumor-infiltrating FOXP3E2$^+$ T_{regs}, we assessed whether their peripheral frequency correlated with the clinical parameters of our BC cohorts, which have been stratified on the basis of histopathological analyses (TNM) into luminal A and B tumors with different survival periods (*69*). First, we evaluated one of the main prognostic markers in BC, the intratumoral Ki67 expression (*70*). We found that the percentage of intratumoral Ki67 was significantly higher in the high– compared to that in the low–E2 PB ratio BC group (20% versus 10%, $P = 0.022$) (Fig. 9A). Furthermore, 74% of the patients with BC with a low E2 PB ratio belonged to the luminal A subgroup [which has a better prognosis than luminal B; (*69*)], while only 43% of patients with BC with a high E2 PB ratio fell in that subgroup (Fig. 9B). Moreover, patients with luminal B BC

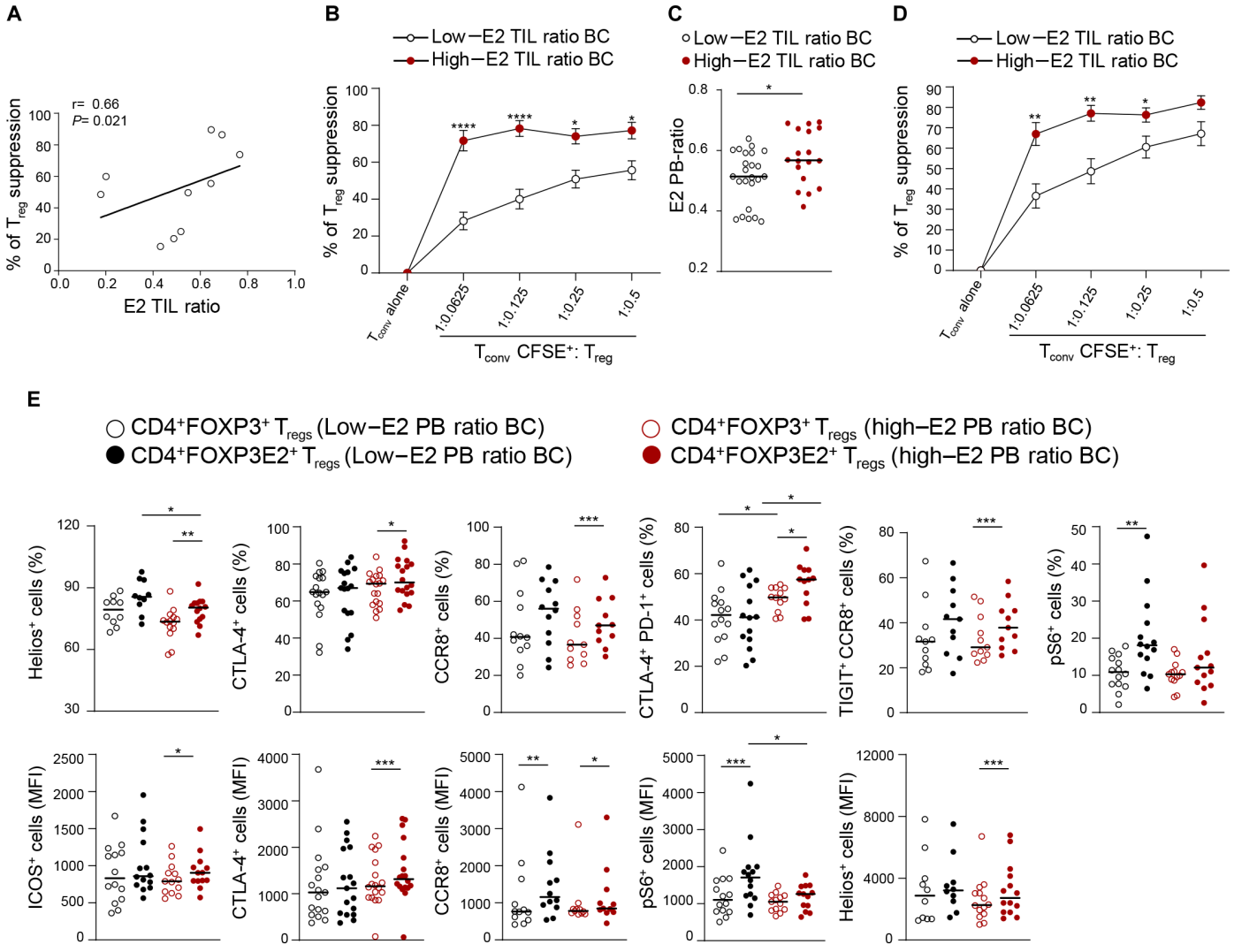

Fig. 8. Increased peripheral T_{reg} suppressive function and IC expression in T_{regs} from patients with BC with a high FOXP3E2 TIL and PB ratio. (**A**) Correlation between the FOXP3E2 TIL ratio (E2 TIL ratio, calculated by flow cytometry quantification of the ratio of $CD4^+FOXP3E2^+/CD4^+FOXP3^+$ T_{regs} from TILs of patients with BC) and the percentage of T_{reg} peripheral suppression from patients with BC ($n = 10$). (**B**) Percentage of suppression of T_{regs} from patients with BC with high ($n = 6$) and low ($n = 6$) E2 TIL ratios at different proportions of T_{regs}/T_{convs}. (**C**) E2 PB ratio from patients with BC with low ($n = 24$) and high ($n = 18$) E2 TIL ratios. (**D**) Percentage of T_{reg} suppression in patients with BC divided into low ($n = 10$) and high ($n = 7$) E2 PB ratio. (**E**) Cumulative data calculated by flow cytometry quantification showing the percentage of $Helios^+$, $CTLA\text{-}4^+$, $CCR8^+$, $CTLA\text{-}4^+PD\text{-}1^+$, $TIGIT^+CCR8^+$, and $pS6^+$ cells and MFI (ICOS, CTLA-4, CCR8, pS6, and Helios) gated on $CD4^+FOXP3^+$ and $CD4^+FOXP3E2^+$ T_{regs} from PB of patients with BC with low (at least $n = 13$) and high (at least $n = 11$) E2 PB ratios. Each symbol shows independent biological samples [(A) to (C) and (E)] or experimental replicates [(B) and (D)]. Data are presented as median values. Statistical analysis was performed by using Wilcoxon and Mann-Whitney *U* test (two tails); $*P \leq 0.05$; $**P \leq 0.01$; $***P \leq 0.005$; $****P \leq 0.0001$.

showed higher PB ratio compared to the luminal A group, and this correlated with stronger suppressive activity (Fig. 9, C and D). Last, we stratified our BC cohort in two clinical-pathological groups with different prognosis (*71*), and we found that E2 PB ratio strictly reflected the overall BC status, as it was significantly increased in the poor-prognosis BC group (0.56 versus 0.51) (Fig. 9E). We show a stronger immunosuppression of peripheral T_{convs} from T_{regs} of the poor-prognosis BC group (Fig. 9F), thus suggesting that an increased percentage of $FOXP3E2^+$ T_{regs} is associated with an enhanced peripheral suppressive function and worse prognosis. Last, we verified the value of FOXP3E2 as prognostic marker in other human cancers and found that, among 26 different cancer types, a high E2 ratio was a prognostic marker associated with lower patient survival for kidney renal papillary cell carcinoma (KIRP), squamous cell carcinoma of the cervix (CESC), and lung adenocarcinoma (LUAD), suggesting a specificity depending on the type of tumor (Fig. 9, G to I, and fig. S12, A to W). Together, our findings suggest that FOXP3E2 might be used as an innovative prognostic marker for BC (Fig. 9J).

DISCUSSION

Women with early-stage BC have an independent risk of recurrence and mortality for at least 20 years after the initial diagnosis with the

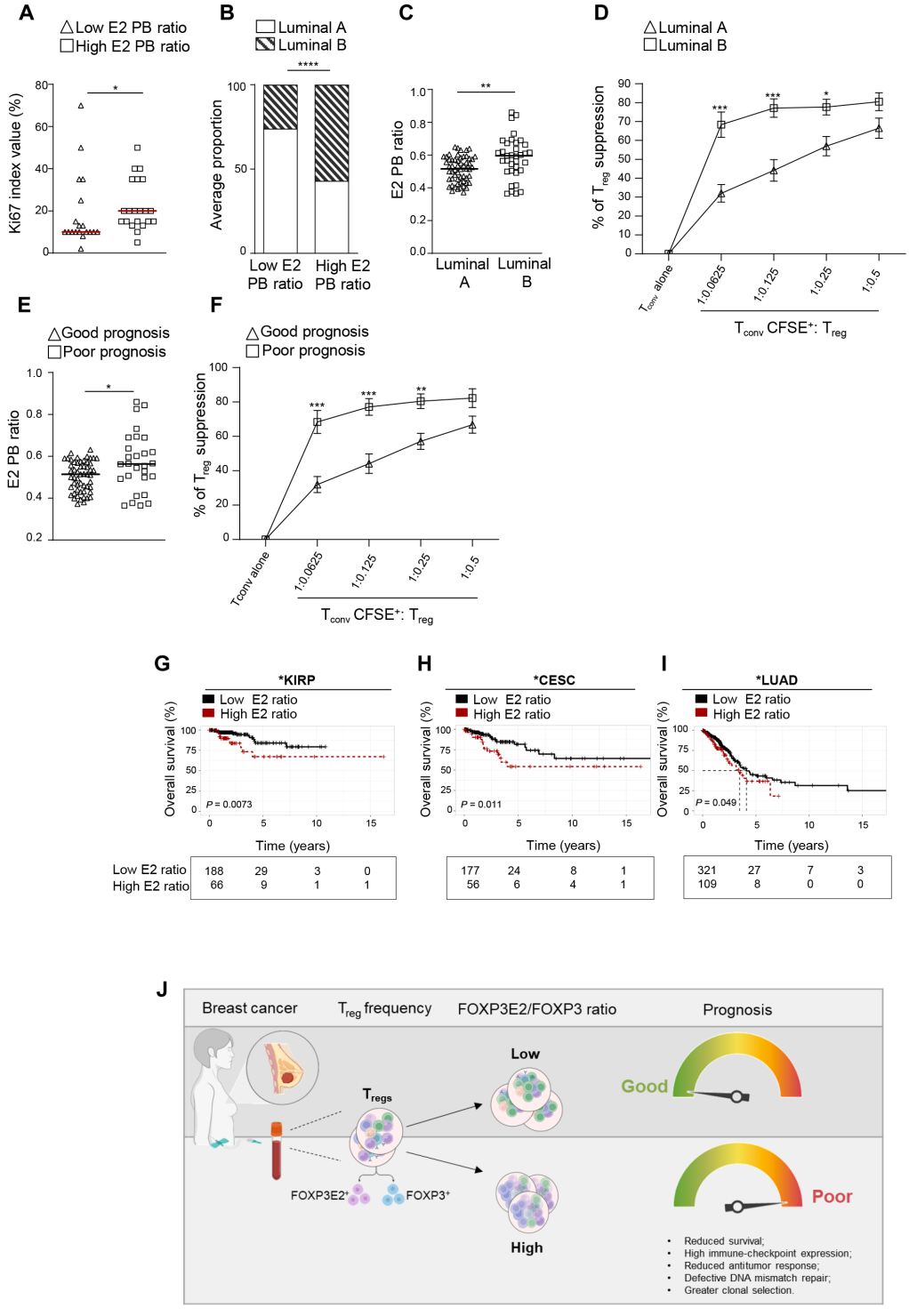

Fig. 9. High blood-derived FOXP3E2$^+$/FOXP3$^+$ ratio associates with worse prognosis and greater immune suppression in patients with HR$^+$BC, and intratumoral FOXP3E2 predicts poor prognosis in KIRP-, CESC-, and LUAD cancer–affected patients. (**A**) Intratumoral Ki67 evaluated in patients with BC with low ($n = 19$) and high ($n = 21$) FOXP3E2 PB ratios. (**B**) Luminal A and luminal B (average proportion) in the low– and high FOXP3E2 PB ratio BC groups. (**C**) FOXP3E2 PB ratio in luminal A ($n = 57$) and luminal B ($n = 35$) BC groups. (**D**) Percentage of suppression in PB-derived T_{regs} isolated from patients with luminal A ($n = 12$) and luminal B ($n = 6$) BC. (**E**) FOXP3E2 PB ratio from patients with BC with good ($n = 54$) and poor ($n = 29$) prognosis. (**F**) Percentage of suppression in PB-derived T_{regs} isolated from patients with BC with good ($n = 13$) and poor ($n = 5$) prognosis. (**G** to **I**) Kaplan-Meier survival curve of KIRP-, CESC-, and LUAD cancer–affected patients stratified into low and high FOXP3E2 ratios according to Q3 value cutoff. (**J**) Schematic summary of the results. Each symbol shows independent biological samples [(A) and (B)] or experimental replicates [(C) to (F)]. Data are presented as median values. Statistical analyses were performed by using Wilcoxon and Mann-Whitney *U* test (two tails) [(A) and (C) to (F)], Fisher's exact test (B), and multivariate Cox regression model reference [(G) to (I)]; $^*P \leq 0.05$; $^{**}P \leq 0.01$; $^{***}P \leq 0.005$; $^{****}P \leq 0.0001$.

greatest impact demonstrated in HR^+ disease, even after 5 years of adjuvant endocrine treatment. To improve survival of patients with BC, an accurate classification of subtypes and the identification of prognostic markers that can predict the course of the disease (e.g., relapse, mortality, and therapeutic response) are needed, alongside with the identification of the underlying molecular pathways.

T_{regs} that express the transcription factor FOXP3 are crucial for maintaining immunological self-tolerance and suppressing the anticancer immune response. The role of distinct T_{reg} subpopulations and their respective functions and interactions within the complex network of the TME have, however, not been fully elucidated (*1*). The composition of intratumoral $FOXP3^+$ T_{regs} is characterized by a subpopulation of highly immune suppressive cells having a distinct gene expression profile, possibly due to the hyperstimulation by tumor-associated antigens (*19*, *31*, *32*). It has been previously reported that, among all $FOXP3^+$ T_{regs}, those expressing the isoforms retaining Exon2 ($FOXP3E2^+$ T_{regs}) display stronger suppressive function and increased lineage stability (*34*, *37*). Notably, although the role of FOXP3 as a master regulator of T_{reg} differentiation and stability is conserved in mouse (*33*, *72*), *Foxp3* gene does not have splicing variants in mouse, making human studies essential to characterize T_{regs} and their function. To date, whether $FOXP3E2^+$ T_{regs} are preferentially enriched within the TME or the PB of patients with cancer and how they correlate with the clinical outcome is still completely unknown.

Here, we investigated the role of T_{regs} in two independent cohorts of patients with newly diagnosed $ER^+PR^+HER2^-$ $(HR)^+$ BC and nonmalignant BF (i.e., 57 patients). Our analyses revealed a different composition of tumor-infiltrating immune cells in BC and nonmalignant tumors, with BC being characterized by a lower $CD8^+/CD4^+$ ratio and a higher frequency of $FOXP3^+$ T_{regs}. Notably, we showed that the $FOXP3E2^+$ T_{reg} subpopulation is increased in the TME of patients with BC compared to that of patients with BF, and a similar enrichment is detected in the PB as well. We further associated $FOXP3E2^+$ T_{reg} enrichment with worst BC prognosis in a wider published cohort of 990 patients with BC (from the TCGA) that also includes $HER2^+$ and triple-negative BC. This was also validated in other human cancers (KIRP, CESC, and LUAD). Overall, our data suggest that FOXP3E2 ratio might be used to develop a blood-based test predictive of prognosis in all BC tumor subtypes and, perhaps, of susceptibility to specific therapies.

The origin of intra-tumoral T_{regs} and their relationship with those circulating in PB remains unclear. Nonetheless, comparing intra-tumoral $FOXP3E2^+$ T_{regs} with those circulating in the PB, we found that both overexpress Helios, a transcription factor that regulates T_{reg} function and stability, suggesting that it might be involved specifically in the differentiation/function of the T_{reg} subset expressing the FOXP3E2 splicing variants. Notably, BC tumors with a high FOXP3E2 ratio showed greater levels of cancer stem cell genes (e.g., WNT3a, NANOGP1, and ESRG) suggesting that this T_{reg} subset might shape the TME to foster cancer stem cell growth or maintenance or vice versa. Notably, some studies have shown that overexpression of WNT3a, ESRG, NANOGP1, NEFL, and PI3K/Akt, which we found in the high–E2 ratio breast tumors, associates with the acquisition of stem cell–like features (*46*–*48*, *73*, *74*), suggesting that there might be an enrichment of CSCs. This is consistent with literature showing that T_{regs} are known to promote cancer stemness (*75*, *76*). It is, therefore, tempting to speculate that a specific cross-talk in-between the tumor and the $FOXP3E2^+$ T_{regs} exists. Gene expression, mutational signature, and clonal evolution analyses showed that FOXP3E2 marks tumors with stronger clonal selection, persistent DNA damage (only ATM-dependent), increased cell survival, and metabolic rewiring induced by hyperactive oncogenic signaling (as PI3K/Akt) (*49*, *77*). Moreover, the lower number of driver genes and the reduced frequency of co-mutations and allelic variants suggest a robust tumor shaping in the high–FOXP3E2 ratio BC group, which could favor the selection of clones associated with increased aggressiveness and drug resistance in cancer (as TP53, PIK3CA, and CDH1) (*4*, *62*, *78*–*81*). Note that chemotherapy and radiation-induced mutagenesis may be accelerated in patients with BC having a deficiency in the DNA MMR system (*82*). Some novel mutated genes may be cancer-driver genes, which means that MMR inactivation can lead to disease progression and therapeutic resistance (*23*). TGCA data mining collectively demonstrates that FOX3E2 expression in the TME is associated with defects in MMR and PI3K/Akt mutations and with lower co-mutation occurrence suggesting higher clonal selection. In addition, FOXP3E2 is associated with stemness and immunomodulatory signatures, suggesting that immune system might contribute to select those stem-like clones evading tumor responses, thus accounting for BC immunological quiescence [minimal response to immunotherapy; (*5*, *50*, *83*)].

Last, our data suggest that $FOXP3E2^+$ T_{regs} may account for higher immunosuppressive function. Notably, we showed that T_{regs} from patients with HR^+ BC with increased FOXP3E2 levels provide stronger suppression of effector cells during functional assays. This is consistent with the increased expression of Helios, ICOS, and IC receptors by T_{reg} immunophenotyping and with the enrichment of a dominant immune gene signature in the patients with BC with a high FOXP3E2 ratio. In addition, known markers of antitumor T cell response (e.g., $CD8^+/T_{reg}$ ratio or CCR8 expression) strongly suggest that this $FOXP3E2^+$ T_{reg} subset is associated with tumor immune escape. Of note, the increased expression of ICOS and lower levels of pS6 suggest that T_{reg} function might be tuned by the mTOR metabolic pathway.

Our overall data suggest that the $FOXP3E2^+$ T_{reg} subpopulation might have a dominant role in cancer evasion/immunosuppression. This might, at least, in part, be mediated by the increased expression of IC co-stimulatory receptors (e.g., CTLA4, PD1, and TIGIT), which represent the targets of currently available immunotherapies that are effective against several malignancies, including BC (e.g., ipilimumab and pembrolizumab) (*1*, *84*–*88*). Notably, the levels of CCR8 are also increased in TIL-$FOXP3E2^+$ T_{regs}. As elevated CCR8 levels in TIL-T_{regs} associate with poor prognosis in several cancer types (*19*, *64*), this could further contribute to $FOXP3E2^+$ T_{reg} retention within the tumor thus amplifying the immunosuppression. In parallel, the TME reinforces the generation of $FOXP3E2^+$ T_{regs} through the release of a CAF-derived chemokine, CXCL12 (*89*, *90*). Intriguingly, CXCL12 has been assigned functions related to epithelial-to-mesenchymal transition, cancer cell stemness, angiogenesis, and immunosuppression (*91*). Moreover, its antagonist, AMD3100, has been shown to inhibit tumor growth and prevent immunosuppression via a selective reduction in the recruitment of $FOXP3^+$ T_{regs} (*65*–*67*). Our results add another piece in the puzzle of the CXCL12/CXCR4 pathway that plays a multifaceted role in the development of highly-specialized niches for stemness, immunosuppression, and other key biological programs contributing to the "metastatic cascade" in the TME (*91*). Overall, our findings led us to hypothesize a central role of the TME that, on one side, promotes cancer stemness to escape immune

surveillance (for example, via hypoxia, inflammation, and DNA damage), whereas, on the other side, promotes immune suppression by inducing highly suppressive FOXP3E2$^+$ T_{regs}. Disentangling the functional interaction between T_{regs} and CSCs will be key in the future to develop novel therapeutic strategies.

Together, our results highlight the importance of considering TIL-FOXP3E2$^+$ T_{regs} as a unique target for improving the actual BC immunotherapeutic strategies. We hypothesized that BC cells may induce (and/or increase recruitment/retention) of FOXP3E2$^+$ T_{regs} through the establishment of a highly immunosuppressive milieu (fig. S13). To this aim, unraveling the specific pathways involved in FOXP3E2$^+$ T_{reg} induction will be instrumental to restrain their generation restoring the tumor-immune responses.

In conclusion, we showed that a high FOXP3E2$^+$/FOXP3$^+$ (E2) ratio in the PB of patients with BC reflects stronger immunosuppression at the tumor site and associates with poor prognosis. Because the accumulation of T_{regs} represents an essential mechanism for cancer immune evasion and a critical barrier to antitumor immunity and immunotherapy, our findings may represent a vital jigsaw piece in the early detection of the BC prognosis puzzle. Furthermore, these results might offer a novel paradigm for developing a "super-targeted" approach that selectively restrains tumor-promoting T_{regs} while preserving a proper peripheral tolerance.

MATERIALS AND METHODS

Participants and study design

The clinical and demographic characteristics of the study cohorts were shown in table S1. Female participants were enrolled after obtaining informed consent. The study has been approved by the Institutional Review Board of the University of Naples "Federico II" (Protocol n. 269/15/ES01). Biological samples were collected by clinicians at the National Cancer Institute – IRCCS "G. Pascale" Foundation (Clinical and Experimental or Oncological Surgery of Senology) and at the Department of General, Oncological, Bariatric and Endocrine-Metabolic Surgery, University of Naples "Federico II," Naples. Patients with BC were naïve to treatment and with definite clinicopathological parameters, including age, TNM stage, histological type and grade [according to World Health Organization (WHO) 2012–2019 and (*92*, *93*)], Ki67 index, ER, progesterone receptor, and HER2 status. For each participant, a detailed past medical history was recorded to exclude intake of glucocorticoids and/or antihistamine drugs in the 2 months preceding the enrolment and previous diagnosis of chronic inflammatory, autoimmune, or other neoplastic diseases. Participants underwent breast surgery or core needle biopsies, collected with ultrasound guidance. Tissue and blood samples were collected before chemotherapy, radiotherapy, endocrine therapy, or any other treatment. Enrolled participants were classified into immunohistochemically defined surrogate molecular subtypes, according to the American Society of Clinical Oncology/College of American Pathologists 2013–2018. Female HDs were matched for age and body mass index and had no history of inflammation, endocrine, or autoimmune disease. The ethnic distribution among the groups was comparable, with all participants being white.

BC and fibroadenoma tissue sample preparation

For the preparation of tissue microarray (TMA) and histologic review, 5-μm sections from each formalin-fixed paraffin-embedded tissue block were stained with hematoxylin and eosin for the identification of tumor areas. IHC analysis was performed on TMA with up to four 1.5-mm cores from primarily the invasive tumor front from each tumor. A review of histologic subtype and grade was performed according to the WHO guidelines (*92*). The diagnosis of ductal carcinoma with medullary characteristics was designated for high-grade tumors with pushing margins and syncytial growth patterns in >75% of the tumor in association with a pronounced lymphoplasmacytic infiltrate (*92*).

Immunohistochemistry

IHC staining was performed on slides from formalin-fixed paraffin-embedded tissues to evaluate the expression of CD3, CD8, FOXP3, and FOXP3E2 markers in BF ($n = 6$) and cancer ($n = 23$) tissues. Paraffin slides were de-paraffinized in xylene and rehydrated through graded alcohols. Antigen retrieval was performed with slides heated in 0.01 M citrate buffer (pH 6.0) in a bath for 20 min at 97°C. After antigen retrieval, the slides allow to cool. The endogenous peroxidase was inactivated with 3% hydrogen. After protein block (5% bovine serum albumin in 1× phosphate-buffered saline), slides were incubated with specific primary antibodies: human anti-CD3 (2GV6) dilution 1:100 (Ventana), human anti-CD8 (CAL66) dilution 1:100 (Roche), human anti-FOXP3 (D2W8E) dilution 1:125 (Cell Signaling Technology), and anti-human FOXP3E2 (150D) dilution 1:125 (BioLegend). The sections were incubated for 1 hour with Novocastra biotinylated secondary antibody (horseradish peroxidase conjugated) and visualized with 3,3′-diaminobenzidine chromogen. Last, the sections were counterstained with hematoxylin and mounted. CD3-, CD8-, FOXP3-, and FOXP3E2-positive nuclei were counted evaluating at least five fields at ×400 magnification. All sections were evaluated in a blinded fashion by two investigators. For each marker, a mean value of up to five cores for each patient was calculated, representing the overall expression of the specific marker.

Breast tissue preparation and cell purification

For the isolation of TILs, dissected tissue fragments from freshly isolated biopsies were transferred in GentleMACS C tubes (Miltenyi Biotec) containing Hanks' balanced salt solution (HBSS) with calcium, magnesium, and sodium bicarbonate and without phenol red (Aurogene) supplemented with collagenase IV (0.5 mg/ml; Sigma-Aldrich), deoxyribonuclease I (50 ng/ml; Worthington), 2% fetal bovine serum (Gibco), and 10% bovine serum albumin (Sigma-Aldrich). Tissue dissociation was made on a GentleMACS Dissociator (Miltenyi Biotec) by using the "h_tumor 01_03" program. Single-cell suspensions were obtained by disrupting the fragments with a syringe plunger over a cell strainer (100 μm) and washing with cold HBSS. Cell suspension was centrifuged at 2700 rpm for 5 min to remove debris, and the cell pellet was resuspended in RPMI 1640 medium for successive evaluations. PB mononuclear cells (PBMCs) from patients with BF and BC and HDs were isolated from blood samples after Ficoll-Hypaque gradient centrifugation (GE Healthcare). T_{regs} ($CD4^+CD25^+CD127^-$) and T_{convs} ($CD4^+CD25^-$) were purified (90 to 95% pure) by using the human $CD4^+CD25^+CD127\ dim^{/-}$ Regulatory T Cell Isolation Kit II (Miltenyi Biotec).

Flow cytometry, proliferation, and CFSE staining

Freshly isolated PBMCs and TILs from patients with BF and BC and female HDs were surface stained with the following monoclonal antibodies (mAbs): allophycocyanin (APC)–H7–conjugated anti-human CD45 (2D1), V500-conjugated anti-human CD4 (RPA-T4), APC-H7–conjugated anti-human CD4 (RPA-T4), phycoerythrin

(PE)–cyanine 7 (Cy7)–conjugated anti-human CD8 (RPA-T8), BV421-conjugated anti-human CD279/PD-1 (EH12.1), and BV421-conjugated anti-human CD198/CCR8 (4333H) (all from BD Biosciences) and PE-Cy7–conjugated anti-human TIGIT (MBCA43) (eBioscience). Thereafter, cells were washed, fixed, and permeabilized (anti-human FOXP3 Staining Set PE; eBioscience) and stained with following mAbs: PE-conjugated anti-human FOXP3 from eBioscience (PCH101, which recognizes all splicing variants through an epitope of the amino terminus of FOXP3), PE-conjugated anti-human FOXP3 from eBioscience (150D/E4, which recognizes FOXP3E2 variants through an epitope present in Exon2 only), APC-conjugated anti-human CD152/CTLA-4 (BNI3) (BD Biosciences), Alexa Fluor 488–conjugated anti-human Helios (22F6), and BV510-conjugated anti-human Ki67 (B56). Cells were analyzed with FACSCanto II (BD Biosciences) and FlowJo software (Tree Star). For T cell proliferation and suppression assays, T_{convs} (2×10^4 cells per well) were stained with the fluorescent dye CFSE at 1 μg/ml (Invitrogen). Flow cytometry analyzing CFSE dilution was performed by gating on $CFSE^+$ cells stimulated for 72 hours in round-bottomed 96-well plates (Corning Falcon) with anti-CD3/anti-CD28 mAb-coated beads (0.2 beads per cell; Thermo Fisher Scientific) alone or cultured with T_{regs} from patients with BC and HDs, respectively.

TS collection and in vitro iT_{reg} generation

TSs were obtained from freshly resected BC tissue biopsies and from MCF10 and MCF7 cell lines. More in detail, single-cell suspensions from BC biopsies were maintained in X-VIVO cell culture medium (X-VIVO 15 Serum-free Hematopoietic Cell Medium, Lonza) for 16 hours, after tissue dissociation (previously described), and, then, TS was collected and used for iT_{reg} generation. Human BC cell lines, MCF10 and MCF7 (CRL-10317 and HTB-22, respectively; ATCC), were grown in Dulbecco's modified Eagle's medium supplemented with penicillin (100 UI/ml), streptomycin (100 μg/ml; Life Technologies), and 10% FBS (Gibco). After 24 hours, TS was collected and used for iT_{reg} generation. To generate iT_{regs}, HD- and BC-T_{convs} were stimulated with Dynabeads coated with mAb to CD3 plus mAb to CD28 (Invitrogen) at a density of 0.1 bead per cell for 24 to 36 hours, as previously described (*35*). Briefly, T_{convs} were cultured (2×10^6 cells/ml) in 96-well plates (Becton-Dickinson, Falcon) with RPMI 1640 medium supplemented with penicillin (100 UI/ml), streptomycin (100 μg/ml; Life Technologies), and either 5% autologous or AB serum (Invitrogen) at a density of 0.1 bead per cell, in the presence or the absence of TS (derived either from freshly resected BC biopsies, MCF10 or MCF7 cell lines). T_{convs} were then harvested and used for immunoblotting or FACS analyses after staining with the following mAbs: APC-H7–conjugated anti-human CD4 (RPA-T4), PE–indodicarbocyanine (Cy5)–conjugated anti-human CD25 (M-A251), PE-conjugated anti-human FOXP3 from eBioscience (PCH101), and PE-conjugated anti-human FOXP3 from eBioscience (150D/E4).

Immunoblot analysis

To generate iT_{regs}, HD- and BC-T_{convs} were stimulated with anti-CD3/anti-CD28 mAbs (0.1 beads per cell) for 24 to 36 hours, as previously described (*35*). Total cell lysates were obtained incubating cells for 20 min at 4°C in radioimmunoprecipitation assay buffer (R0278; Sigma-Aldrich) plus SIGMAFAST Protease Inhibitor (S8820; Sigma-Aldrich) and Sigma Phosphatase Inhibitor (P5726; Sigma-Aldrich), and immunoblot analyses were performed as described (*35*). The mAbs used were the following: anti-FOXP3 (clone PCH101), anti-FOXP3E2 (clone 150D/E4) (1:500 dilution; all from Thermo Fisher Scientific), and anti-extracellular signal–regulated kinase 1/2 (ERK 1/2) (H72) (1:1000 dilution; Santa Cruz Biotechnology) to normalize the amount of loaded protein. All filters were quantified by densitometry using ImageJ software (National Institutes of Health). We scanned at least two films with different exposures for each protein detected. Results were calculated and normalized to densitometry of ERK 1/2 and are presented relative to the results obtained for 24- and 36-hour TCR-stimulated T_{convs}.

Human chemokine and cytokine assay

TSs were collected from BC biopsies and screened for 6Ckine/CCL21, BCA-1/CXCL13, CTACK/CCL27, ENA-78/CXCL5, Eotaxin/CCL11, Eotaxin-2/CCL24, Eotaxin-3/CCL26, Fractalkine/CX3CL1, GCP-2/CXCL6, granulocyte-macrophage colony-stimulating factor (GM-CSF), Gro-α/CXCL1, Gro-β/CXCL2, I-309/CCL1, interferon-γ (IFN-γ), interleukin-1β (IL-1β), IL-2, IL-4, IL-6, IL-8/CXCL8, IL-10, IL-16, IP-10/CXCL10, I-TAC/CXCL11, MCP-1/CCL2, MCP-2/CCL8, MCP-3/CCL7, MCP-4/CCL13, MDC/CCL22, migration inhibition factor (MIF), MIG/CXCL9 MIP-1α/CCL3, MIP-1δ/CCL15, MIP-3α/CCL20, MIP-3β/CCL19, MPIF-1/CCL23, SCYB16/CXCL16, SDF-1α$^+$β/CXCL12, TARC/CCL17, TECK/CCL25, and tumor necrosis factor–α (TNF-α) using the Bio-Plex multiplex Human Chemokine 40-plex Panel (Bio-Rad) according to the manufacturer's protocol.

Systematic transcript variant analysis in public databases

The FOXP3-spliced variant sequences were assessed in UCSC Genome Browser on Human (GRCh37/hg19) (*94*) databases. The schematic diagram of the FOXP3 variant structures is reported in fig. S1E.

TCGA database analyses

FOXP3 splicing variant expression data are derived from TSVdb web tool (www.tsvdb.com) and are reported as normalized RNA-seq by expectation maximization (RSEM) values. Samples with unreported and/or missing clinical data were removed. The FOXP3E2/FOXP3 ratio was calculated using GRCh37/hg19 coordinates chrX:49,114,121-49,114,225 and chrX:49,109,587-49,109,663 that recognize, respectively, the FOXP3 splicing variants containing Exon2 and Exon9 (being this last common to all transcripts).

Kaplan-Meier survival plot

Overall survival analysis was conducted using only patients with survival and gene expression data from TSVdb. Samples were categorized using Cox proportional hazards regression into two groups on the basis of either on the mean RSEM value (high expression ≥ Q2 and low expression < Q2) or on the upper quartile RSEM value (high expression ≥ Q3 and low expression < Q3). The Kaplan-Meier survival plots were generated using R packages: "survival and survminer." The survival curves of samples with high and low gene expression were compared by log-rank test, and data groups with a P value of <0.05 were considered statistically significant.

TCGA RNA-seq analysis

Primary BC (n = 990) and NT (n = 112) RNA-seq data counts were downloaded from the TCGA-BRCA project (available online at https://portal.gdc.cancer.gov/projects/TCGA-BRCA). Further analysis and visualizations of the processed data were performed in R and Bioconductor. For differential expression analyses between

high (n = 248)– and low (n = 742)–ratio BC groups, counts were normalized using the size factor normalization technique available in DESeq2 and an absolute $\log_2$ fold change > 0.5 and P adj. of < 0.001. We used the online tools RDAVIDWebService (*95*) and GOplot (*96*) to identify GO Biological Processes overrepresented and to prepare circular composition overview. We performed a statistical overrepresentation test using default parameters. GO terms were considered overrepresented only if FDR-corrected P values were below <0.05. Then, ClusterProfiler v.4.6 and Enrichplot v.1.19.0.01 were used for GSEA and plotting (*49*, *97*). DNA MMR gene expressions were obtained by comparing the low (n = 742)– and high (n = 248)–ratio BC groups and filtering the normalized count matrix.

Tumor immune microenvironment cell composition analysis

Immune and stroma composition analysis of patients with BC with low (n = 735) and high (n = 248) FOXP3E2 ratios (tumor immune microenvironment deconvolution) was performed using the online tool TimeDB (*61*) on the basis of DEGs obtained from TCGA-BRCA RNA-seq analysis.

Mutation enrichment analysis

Variants were obtained from TCGA-BRCA whole exome sequencing (WES) using the TCGAbiolinks R package (*98*) to identify differentially mutated genes in low (n = 650)– and high (n = 211)–ratio BC groups. Analysis (variants number, somatic interactions, tumor mutational burden, APOBEC enrichments, and signatures detection) and visualization of mutations were performed using the Maftools R package (*99*). Contributions of mutational signatures in COSMIC (*100*) were determined in each sample using nonnegative matrix factorization provided by the NMF v1.8.0 R package (*101*) using a P value of <0.001. The contributions of identified COSMIC mutational signatures were confirmed using the "mutSignatures" R package. The variant allelic frequency of low– and high–FOXP3E2 ratio groups was compared using the ClonEvol tool in R (https://github.com/hdng/clonevol) using default settings. Each point in a different color represents an independent variant across clusters and groups.

dN/dS analysis of mutations

dN/dS analysis was performed using the dNdScv function from the R package "dNdScv" (https://github.com/im3sanger/dndscv) using default settings except for the following arguments: max_muts_per_gene_per_sample = Inf, use_indel_sites = T, and max_coding_muts_per_sample = Inf. Genes were considered to have evidence of positive selection if the reported dN/dS q value was <0.05 for missense mutations, truncating variants, all substitutions, or indels. Network analysis was carried out using the igraph package in R and co-occurrence genes from Maftools with a P value of <0.05.

Neoantigen analysis

Neoantigen counts are available from Thorsson *et al.* (*102*) (supplementary files: TCGA_PCA.mc3.v0.2.8.CONTROLLED.filtered.sample_neoantigens.10062017.tsv, gdc.cancer.gov/about-data/publications/panimmune).

Differentially methylated regions

Differentially methylated regions were calculated using the normalized beta values (methylation values ranging from 0.0 to 1.0) obtained from TCGA-BRCA Illumina Human Methylation 450 downloaded through TCGAbiolinks R package. To compare low (n = 524)– and high (n = 194)–ratio BC groups, we used the Wilcoxon test with the adjusted Benjamini-Hochberg method. The default parameters were set to require a minimum absolute beta-value difference of 0.2 and a P value adjusted of <0.01.

RPPA analysis

Proteomic analyses were performed using level 4 ($\log_2$ transformed with loading and batch corrected) RPPA dataset from the TCGA-BRCA study downloaded from The Cancer Proteome Atlas portal (https://tcpaportal.org/tcpa/). For differential protein expression analysis between high (n = 248)– and low (n = 742)–ratio BC groups, RPPA relative fluorescence intensity (RFI) values were compared using an analysis of variance (ANOVA) FDR P-value threshold of less than 0.05. The data were then scaled on the basis of average RFI threshold for each protein to extract up-regulated (red) and down-regulated (green) probes of the high-ratio BC group. Metascape was used to perform the enrichment analysis of the differentially expressed probes. The data were displayed as median values.

Statistical analysis

Statistical analyses were performed using GraphPad program (Abacus Concepts) and R packages. Results were expressed as median and interquartile range. The nonparametric Mann-Whitney U test, the Wilcoxon matched-pairs signed-rank test, and the t test were used. Correlations were computed with a nonparametric Spearman r correlation test, overall survival with a log-rank test, and hazard ratio with multivariate Cox regression model reference. A two-tailed P value of <0.05 was considered statistically significant.

Supplementary Materials

This PDF file includes:

Figs. S1 to S13
Table S1

REFERENCES AND NOTES

1. F. Shan, A. Somasundaram, T. C. Bruno, C. J. Workman, D. A. A. Vignali, Therapeutic targeting of regulatory T cells in cancer. *Trends Cancer* **8**, 944–961 (2022).
2. Y. Togashi, K. Shitara, H. Nishikawa, Regulatory T cells in cancer immunosuppression—Implications for anticancer therapy. *Nat. Rev. Clin. Oncol.* **16**, 356–371 (2019).
3. G. P. Dunn, A. T. Bruce, H. Ikeda, L. J. Old, R. D. Schreiber, Cancer immunoediting: From immunosurveillance to tumor escape. *Nat. Immunol.* **3**, 991–998 (2002).
4. J. S. O'Donnell, M. W. L. Teng, M. J. Smyth, Cancer immunoediting and resistance to T cell-based immunotherapy. *Nat. Rev. Clin. Oncol.* **16**, 151–167 (2019).
5. J. Blanco-Heredia, C. A. Souza, J. L. Trincado, M. Gonzalez-Cao, S. Goncalves-Ribeiro, S. R. Gil, D. Pravdyvets, S. Cedeno, M. Callari, A. Marra, A. M. Gazzo, B. Weigelt, F. Pareja, T. Vougiouklakis, A. A. Jungbluth, R. Rosell, C. Brander, F. Tresserra, J. S. Reis-Filho, D. G. Tiezzi, N. de la Iglesia, H. Heyn, L. De Mattos-Arruda, Converging and evolving immuno-genomic routes toward immune escape in breast cancer. *Nat. Commun.* **15**, 1302 (2024).
6. N. McGranahan, R. Rosenthal, C. T. Hiley, A. J. Rowan, T. B. K. Watkins, G. A. Wilson, N. J. Birkbak, S. Veeriah, P. Van Loo, J. Herrero, C. Swanton, TRACERx Consortium, Allele-specific HLA loss and immune escape in lung cancer evolution. *Cell* **171**, 1259–1271 e11 (2017).
7. S. Adams, P. Schmid, H. S. Rugo, E. P. Winer, D. Loirat, A. Awada, D. W. Cescon, H. Iwata, M. Campone, R. Nanda, R. Hui, G. Curigliano, D. Toppmeyer, J. O'Shaughnessy, S. Loi, S. Paluch-Shimon, A. R. Tan, D. Card, J. Zhao, V. Karantza, J. Cortes, Pembrolizumab monotherapy for previously treated metastatic triple-negative breast cancer: Cohort A of the phase II KEYNOTE-086 study. *Ann. Oncol.* **30**, 397–404 (2019).
8. M. E. Gatti-Mays, J. M. Balko, S. R. Gameiro, H. D. Bear, S. Prabhakaran, J. Fukui, M. L. Disis, R. Nanda, J. L. Gulley, K. Kalinsky, H. Abdul Sater, J. A. Sparano, D. Cescon, D. B. Page,

H. McArthur, S. Adams, E. A. Mittendorf, If we build it they will come: Targeting the immune response to breast cancer. *NPJ Breast Cancer* **5**, 37 (2019).
9. R. R. Gomis, S. Gawrzak, Tumor cell dormancy. *Mol. Oncol.* **11**, 62–78 (2017).
10. T. G. Karrison, D. J. Ferguson, P. Meier, Dormancy of mammary carcinoma after mastectomy. *J. Natl. Cancer Inst.* **91**, 80–85 (1999).
11. R. Demicheli, E. Biganzoli, I. Ardoino, P. Boracchi, D. Coradini, M. Greco, A. Moliterni, M. Zambetti, P. Valagussa, I. D. Gukas, G. Bonadonna, Recurrence and mortality dynamics for breast cancer patients undergoing mastectomy according to estrogen receptor status: Different mortality but similar recurrence. *Cancer Sci.* **101**, 826–830 (2010).
12. M. Colleoni, Z. Sun, K. N. Price, P. Karlsson, J. F. Forbes, B. Thurlimann, L. Gianni, M. Castiglione, R. D. Gelber, A. S. Coates, A. Goldhirsch, Annual hazard rates of recurrence for breast cancer during 24 years of follow-up: Results from the international breast cancer study group trials I to V. *J. Clin. Oncol.* **34**, 927–935 (2016).
13. P. F. Denoix, Nomenclature and classification of cancers based on an atlas. *Acta Unio Int. Contra Cancrum* **9**, 769–771 (1953).
14. A. F. Vieira, F. Schmitt, An update on breast cancer multigene prognostic tests—Emergent clinical biomarkers. *Front. Med.* **5**, 248 (2018).
15. R. N. Pedersen, B. O. Esen, L. Mellemkjaer, P. Christiansen, B. Ejlertsen, T. L. Lash, M. Norgaard, D. Cronin-Fenton, The incidence of breast cancer recurrence 10-32 years after primary diagnosis. *J. Natl. Cancer Inst.* **114**, 391–399 (2022).
16. H. Pan, R. Gray, J. Braybrooke, C. Davies, C. Taylor, P. McGale, R. Peto, K. I. Pritchard, J. Bergh, M. Dowsett, D. F. Hayes, EBCTCG, 20-Year risks of breast-cancer recurrence after stopping endocrine therapy at 5 years. *N. Engl. J. Med.* **377**, 1836–1846 (2017).
17. R. L. Siegel, K. D. Miller, A. Jemal, Cancer statistics, 2020. *CA Cancer J. Clin.* **70**, 7–30 (2020).
18. G. L. Beatty, W. L. Gladney, Immune escape mechanisms as a guide for cancer immunotherapy. *Clin. Cancer Res.* **21**, 687–692 (2015).
19. M. De Simone, A. Arrigoni, G. Rossetti, P. Gruarin, V. Ranzani, C. Politano, R. J. P. Bonnal, E. Provasi, M. L. Sarnicola, I. Panzeri, M. Moro, M. Crosti, S. Mazzara, V. Vaira, S. Bosari, A. Palleschi, L. Santambrogio, G. Bovo, N. Zucchini, M. Totis, L. Gianotti, G. Cesana, R. A. Perego, N. Maroni, A. P. Ceretti, E. Opocher, R. De Francesco, J. Geginat, H. G. Stunnenberg, S. Abrignani, M. Pagani, Transcriptional landscape of human tissue lymphocytes unveils uniqueness of tumor-infiltrating T regulatory cells. *Immunity* **45**, 1135–1147 (2016).
20. B. Shang, Y. Liu, S. J. Jiang, Y. Liu, Prognostic value of tumor-infiltrating FoxP3$^+$ regulatory T cells in cancers: A systematic review and meta-analysis. *Sci. Rep.* **5**, 15179 (2015).
21. A. Tanaka, S. Sakaguchi, Regulatory T cells in cancer immunotherapy. *Cell Res.* **27**, 109–118 (2017).
22. R. Saleh, E. Elkord, FoxP3$^+$ T regulatory cells in cancer: Prognostic biomarkers and therapeutic targets. *Cancer Lett.* **490**, 174–185 (2020).
23. S. Liu, W. D. Foulkes, S. Leung, D. Gao, S. Lau, Z. Kos, T. O. Nielsen, Prognostic significance of FOXP3+ tumor-infiltrating lymphocytes in breast cancer depends on estrogen receptor and human epidermal growth factor receptor-2 expression status and concurrent cytotoxic T-cell infiltration. *Breast Cancer Res.* **16**, 432 (2014).
24. S. A. Perez, M. V. Karamouzis, D. V. Skarlos, A. Ardavanis, N. N. Sotiriadou, E. G. Iliopoulou, M. L. Salagianni, G. Orphanos, C. N. Baxevanis, G. Rigatos, M. Papamichail, CD4$^+$CD25$^+$ regulatory T-cell frequency in HER-2/neu (HER)-positive and HER-negative advanced-stage breast cancer patients. *Clin. Cancer Res.* **13**, 2714–2721 (2007).
25. R. J. deLeeuw, S. E. Kost, J. A. Kakal, B. H. Nelson, The prognostic value of FoxP3$^+$ tumor-infiltrating lymphocytes in cancer: A critical review of the literature. *Clin. Cancer Res.* **18**, 3022–3029 (2012).
26. J. Stenstrom, I. Hedenfalk, C. Hagerling, Regulatory T lymphocyte infiltration in metastatic breast cancer-an independent prognostic factor that changes with tumor progression. *Breast Cancer Res.* **23**, 27 (2021).
27. K. Kos, M. A. Aslam, R. van de Ven, M. D. Wellenstein, W. Pieters, A. van Weverwijk, D. E. M. Duits, K. van Pul, C. S. Hau, K. Vrijland, D. Kaldenbach, E. A. M. Raeven, S. A. Quezada, R. Beyaert, H. Jacobs, T. D. de Gruijl, K. E. de Visser, Tumor-educated T$_{regs}$ drive organ-specific metastasis in breast cancer by impairing NK cells in the lymph node niche. *Cell Rep.* **38**, 110447 (2022).
28. N. R. West, S. E. Kost, S. D. Martin, K. Milne, R. J. Deleeuw, B. H. Nelson, P. H. Watson, Tumour-infiltrating FOXP3$^+$ lymphocytes are associated with cytotoxic immune responses and good clinical outcome in oestrogen receptor-negative breast cancer. *Br. J. Cancer* **108**, 155–162 (2013).
29. G. Plitas, C. Konopacki, K. Wu, P. D. Bos, M. Morrow, E. V. Putintseva, D. M. Chudakov, A. Y. Rudensky, Regulatory T cells exhibit distinct features in human breast cancer. *Immunity* **45**, 1122–1134 (2016).
30. J. G. Tate, S. Bamford, H. C. Jubb, Z. Sondka, D. M. Beare, N. Bindal, H. Boutselakis, C. G. Cole, C. Creatore, E. Dawson, P. Fish, B. Harsha, C. Hathaway, S. C. Jupe, C. Y. Kok, K. Noble, L. Ponting, C. C. Ramshaw, C. E. Rye, H. E. Speedy, R. Stefancsik, S. L. Thompson, S. Wang, S. Ward, P. J. Campbell, S. A. Forbes, COSMIC: The catalogue of somatic mutations in cancer. *Nucleic Acids Res.* **47**, D941–D947 (2019).
31. H. Nakagawa, J. M. Sido, E. E. Reyes, V. Kiers, H. Cantor, H. J. Kim, Instability of Helios-deficient Tregs is associated with conversion to a T-effector phenotype and enhanced antitumor immunity. *Proc. Natl. Acad. Sci. U.S.A.* **113**, 6248–6253 (2016).
32. M. J. Watson, P. D. A. Vignali, S. J. Mullett, A. E. Overacre-Delgoffe, R. M. Peralta, S. Grebinoski, A. V. Menk, N. L. Rittenhouse, K. DePeaux, R. D. Whetstone, D. A. A. Vignali, T. W. Hand, A. C. Poholek, B. M. Morrison, J. D. Rothstein, S. G. Wendell, G. M. Delgoffe, Metabolic support of tumour-infiltrating regulatory T cells by lactic acid. *Nature* **591**, 645–651 (2021).
33. R. K. W. Mailer, Alternative splicing of FOXP3—Virtue and vice. *Front. Immunol.* **9**, 530 (2018).
34. N. Goda, S. Sasada, H. Shigematsu, N. Masumoto, K. Arihiro, H. Nishikawa, S. Sakaguchi, M. Okada, T. Kadoya, The ratio of CD8 + lymphocytes to tumor-infiltrating suppressive FOXP3 + effector regulatory T cells is associated with treatment response in invasive breast cancer. *Discov. Oncol.* **13**, 27 (2022).
35. V. De Rosa, M. Galgani, A. Porcellini, A. Colamatteo, M. Santopaolo, C. Zuchegna, A. Romano, S. De Simone, C. Procaccini, C. La Rocca, P. B. Carrieri, G. T. Maniscalco, M. Salvetti, M. C. Buscarinu, A. Franzese, E. Mozzillo, A. La Cava, G. Matarese, Glycolysis controls the induction of human regulatory T cells by modulating the expression of FOXP3 exon 2 splicing variants. *Nat. Immunol.* **16**, 1174–1184 (2015).
36. S. Junius, A. V. Mavrogiannis, P. Lemaitre, M. Gerbaux, F. Staels, V. Malviya, O. Burton, V. Gergelits, K. Singh, R. Y. Tito Tadeo, J. Raes, S. Humblet-Baron, A. Liston, S. M. Schlenner, Unstable regulatory T cells, enriched for naive and Nrp1^{neg} cells, are purged after fate challenge. *Sci. Immunol.* **6**, eabe4723 (2021).
37. J. Du, Q. Wang, S. Yang, S. Chen, Y. Fu, S. Spath, P. Domeier, D. Hagin, S. Anover-Sombke, M. Haouili, S. Liu, J. Wan, L. Han, J. Liu, L. Yang, N. Sangani, Y. Li, X. Lu, S. C. Janga, M. H. Kaplan, T. R. Torgerson, S. F. Ziegler, B. Zhou, FOXP3 exon 2 controls T$_{reg}$ stability and autoimmunity. *Sci. Immunol.* **7**, eabo5407 (2022).
38. L. Demir, S. Yigit, H. Ellidokuz, C. Erten, I. Somali, Y. Kucukzeybek, A. Alacacioglu, S. Cokmert, A. Can, M. Akyol, A. Dirican, V. Bayoglu, A. A. Sari, M. O. Tarhan, Predictive and prognostic factors in locally advanced breast cancer: effect of intratumoral FOXP3+ Tregs. *Clin. Exp. Metastasis* **30**, 1047–1062 (2013).
39. S. Garaud, C. Gu-Trantien, J. N. Lodewyckx, A. Boisson, P. De Silva, L. Buisseret, E. Migliori, M. Libin, C. Naveaux, H. Duvillier, K. Willard-Gallo, A simple and rapid protocol to non-enzymatically dissociate fresh human tissues for the analysis of infiltrating lymphocytes. *J. Vis. Exp.* , 52392 (2014).
40. W. Sun, T. Duan, P. Ye, K. Chen, G. Zhang, M. Lai, H. Zhang, TSVdb: A web-tool for TCGA splicing variants analysis. *BMC Genomics* **19**, 405 (2018).
41. D. O. Croci, M. F. Zacarias Fluck, M. J. Rico, P. Matar, G. A. Rabinovich, O. G. Scharovsky, Dynamic cross-talk between tumor and immune cells in orchestrating the immunosuppressive network at the tumor microenvironment. *Cancer Immunol. Immunother.* **56**, 1687–1700 (2007).
42. T. L. Whiteside, The tumor microenvironment and its role in promoting tumor growth. *Oncogene* **27**, 5904–5912 (2008).
43. M. Kanehisa, S. Goto, KEGG: Kyoto encyclopedia of genes and genomes. *Nucleic Acids Res.* **28**, 27–30 (2000).
44. P. Jayachandran, F. Battaglin, C. Strelez, A. Lenz, S. Algaze, S. Soni, J. H. Lo, Y. Yang, J. Millstein, W. Zhang, J. C. Shih, J. Lu, S. M. Mumenthaler, D. Spicer, J. Neman, E. T. R. Torres, H. J. Lenz, Breast cancer and neurotransmitters: Emerging insights on mechanisms and therapeutic directions. *Oncogene* **42**, 627–637 (2023).
45. I. Bozic, T. Antal, H. Ohtsuki, H. Carter, D. Kim, S. Chen, R. Karchin, K. W. Kinzler, B. Vogelstein, M. A. Nowak, Accumulation of driver and passenger mutations during tumor progression. *Proc. Natl. Acad. Sci. U.S.A.* **107**, 18545–18550 (2010).
46. E. Lee, J. Yang, M. Ku, N. H. Kim, Y. Park, C. B. Park, J. S. Suh, E. S. Park, J. I. Yook, G. B. Mills, Y. M. Huh, J. H. Cheong, Metabolic stress induces a Wnt-dependent cancer stem cell-like state transition. *Cell Death Dis.* **6**, e1805 (2015).
47. K. Takahashi, M. Nakamura, C. Okubo, Z. Kliesmete, M. Ohnuki, M. Narita, A. Watanabe, M. Ueda, Y. Takashima, I. Hellmann, S. Yamanaka, The pluripotent stem cell-specific transcript ESRG is dispensable for human pluripotency. *PLOS Genet.* **17**, e1009587 (2021).
48. K. Maskalenka, G. Alagoz, F. Krueger, J. Wright, M. Rostovskaya, A. Nakhuda, A. Bendall, C. Krueger, S. Walker, A. Scally, P. J. Rugg-Gunn, NANOGP1, a tandem duplicate of NANOG, exhibits partial functional conservation in human naive pluripotent stem cells. *Development* **150**, dev201155 (2023).
49. T. Wu, E. Hu, S. Xu, M. Chen, P. Guo, Z. Dai, T. Feng, L. Zhou, W. Tang, L. Zhan, X. Fu, S. Liu, X. Bo, G. Yu, clusterProfiler 4.0: A universal enrichment tool for interpreting omics data. *Innovation (Camb)* **2**, 100141 (2021).
50. L. Beumers, E. I. Vlachavas, S. Borgoni, L. Schwarzmuller, L. Penso-Dolfin, B. E. Michels, E. Sofyali, S. Burmester, D. Heiss, H. Wilhelm, Y. Yarden, D. Helm, R. Will, A. Goncalves, S. Wiemann, Clonal heterogeneity in ER+ breast cancer reveals the proteasome and PKC as potential therapeutic targets. *NPJ Breast Cancer* **9**, 97 (2023).
51. M. Karami Fath, M. Ebrahimi, E. Nourbakhsh, A. Zia Hazara, A. Mirzaei, S. Shafieyari, A. Salehi, M. Hoseinzadeh, Z. Payandeh, G. Barati, PI3K/Akt/mTOR signaling pathway in cancer stem cells. *Pathol. Res. Pract.* **237**, 154010 (2022).

52. Y. He, M. M. Sun, G. G. Zhang, J. Yang, K. S. Chen, W. W. Xu, B. Li, Targeting PI3K/Akt signal transduction for cancer therapy. *Signal Transduct. Target. Ther.* **6**, 425 (2021).
53. I. Martincorena, K. M. Raine, M. Gerstung, K. J. Dawson, K. Haase, P. Van Loo, H. Davies, M. R. Stratton, P. J. Campbell, Universal patterns of selection in cancer and somatic tissues. *Cell* **171**, 1029–1041.e21 (2017).
54. Y. Zhang, P. Naderi Yeganeh, H. Zhang, S. Y. Wang, Z. Li, B. Gu, D. J. Lee, Z. Zhang, A. Ploumakis, M. Shi, H. Wu, E. L. Greer, W. Hide, J. Lieberman, Tumor editing suppresses innate and adaptive antitumor immunity and is reversed by inhibiting DNA methylation. *Nat. Immunol.* **25**, 1858–1870 (2024).
55. S. Nik-Zainal, H. Davies, J. Staaf, M. Ramakrishna, D. Glodzik, X. Zou, I. Martincorena, L. B. Alexandrov, S. Martin, D. C. Wedge, P. Van Loo, Y. S. Ju, M. Smid, A. B. Brinkman, S. Morganella, M. R. Aure, O. C. Lingjaerde, A. Langerod, M. Ringner, S. M. Ahn, S. Boyault, J. E. Brock, A. Broeks, A. Butler, C. Desmedt, L. Dirix, S. Dronov, A. Fatima, J. A. Foekens, M. Gerstung, G. K. Hooijer, S. J. Jang, D. R. Jones, H. Y. Kim, T. A. King, S. Krishnamurthy, H. J. Lee, J. Y. Lee, Y. Li, S. McLaren, A. Menzies, V. Mustonen, S. O'Meara, I. Pauporte, X. Pivot, C. A. Purdie, K. Raine, K. Ramakrishnan, F. G. Rodriguez-Gonzalez, G. Romieu, A. M. Sieuwerts, P. T. Simpson, R. Shepherd, L. Stebbings, O. A. Stefansson, J. Teague, S. Tommasi, I. Treilleux, G. G. Van den Eynden, P. Vermeulen, A. Vincent-Salomon, L. Yates, C. Caldas, L. van't Veer, A. Tutt, S. Knappskog, B. K. Tan, J. Jonkers, A. Borg, N. T. Ueno, C. Sotiriou, A. Viari, P. A. Futreal, P. J. Campbell, P. N. Span, S. Van Laere, S. R. Lakhani, J. E. Eyfjord, A. M. Thompson, E. Birney, H. G. Stunnenberg, M. J. van de Vijver, J. W. Martens, A. L. Borresen-Dale, A. L. Richardson, G. Kong, G. Thomas, M. R. Stratton, Landscape of somatic mutations in 560 breast cancer whole-genome sequences. *Nature* **534**, 47–54 (2016).
56. S. Nik-Zainal, P. Van Loo, D. C. Wedge, L. B. Alexandrov, C. D. Greenman, K. W. Lau, K. Raine, D. Jones, J. Marshall, M. Ramakrishna, A. Shlien, S. L. Cooke, J. Hinton, A. Menzies, L. A. Stebbings, C. Leroy, M. Jia, R. Rance, L. J. Mudie, S. J. Gamble, P. J. Stephens, S. McLaren, P. S. Tarpey, E. Papaemmanuil, H. R. Davies, I. Varela, D. J. McBride, G. R. Bignell, K. Leung, A. P. Butler, J. W. Teague, S. Martin, G. Jonsson, O. Mariani, S. Boyault, P. Miron, A. Fatima, A. Langerod, S. A. Aparicio, A. Tutt, A. M. Sieuwerts, A. Borg, G. Thomas, A. V. Salomon, A. L. Richardson, A. L. Borresen-Dale, P. A. Futreal, M. R. Stratton, P. J. Campbell, Breast Cancer Working Group of the International Cancer Genome Consortium, The life history of 21 breast cancers. *Cell* **149**, 994–1007 (2012).
57. M. B. Burns, L. Lackey, M. A. Carpenter, A. Rathore, A. M. Land, B. Leonard, E. W. Refsland, D. Kotandeniya, N. Tretyakova, J. B. Nikas, D. Yee, N. A. Temiz, D. E. Donohue, R. M. McDougle, W. L. Brown, E. K. Law, R. S. Harris, APOBEC3B is an enzymatic source of mutation in breast cancer. *Nature* **494**, 366–370 (2013).
58. L. B. Alexandrov, S. Nik-Zainal, D. C. Wedge, S. A. Aparicio, S. Behjati, A. V. Biankin, G. R. Bignell, N. Bolli, A. Borg, A. L. Borresen-Dale, S. Boyault, B. Burkhardt, A. P. Butler, C. Caldas, H. R. Davies, C. Desmedt, R. Eils, J. E. Eyfjord, J. A. Foekens, M. Greaves, F. Hosoda, B. Hutter, T. Ilicic, S. Imbeaud, M. Imielinski, N. Jager, D. T. Jones, D. Jones, S. Knappskog, M. Kool, S. R. Lakhani, C. Lopez-Otin, S. Martin, N. C. Munshi, H. Nakamura, P. A. Northcott, M. Pajic, E. Papaemmanuil, A. Paradiso, J. V. Pearson, X. S. Puente, K. Raine, M. Ramakrishna, A. L. Richardson, J. Richter, P. Rosenstiel, M. Schlesner, T. N. Schumacher, P. N. Span, J. W. Teague, Y. Totoki, A. N. Tutt, R. Valdes-Mas, M. M. van Buuren, L. 't van Veer, A. Vincent-Salomon, N. Waddell, L. R. Yates, Australian Pancreatic Cancer Genome Initiative, ICGC Breast Cancer Consortium, ICGC MMML-Seq Consortium, ICGC PedBrain, J. Zucman-Rossi, P. A. Futreal, U. McDermott, P. Lichter, M. Meyerson, S. M. Grimmond, R. Siebert, E. Campo, T. Shibata, S. M. Pfister, P. J. Campbell, M. R. Stratton, Signatures of mutational processes in human cancer. *Nature* **500**, 415–421 (2013).
59. S. Haricharan, N. Punturi, P. Singh, K. R. Holloway, M. Anurag, J. Schmelz, C. Schmidt, J. T. Lei, V. Suman, K. Hunt, J. A. Olson Jr., J. Hoog, S. Li, S. Huang, D. P. Edwards, S. M. Kavuri, M. N. Bainbridge, C. X. Ma, M. J. Ellis, Loss of MutL disrupts CHK2-dependent cell-cycle control through CDK4/6 to promote intrinsic endocrine therapy resistance in primary breast cancer. *Cancer Discov.* **7**, 1168–1183 (2017).
60. M. Anurag, N. Punturi, J. Hoog, M. N. Bainbridge, M. J. Ellis, S. Haricharan, Comprehensive profiling of DNA repair defects in breast cancer identifies a novel class of endocrine therapy resistance drivers. *Clin. Cancer Res.* **24**, 4887–4899 (2018).
61. X. Wang, L. Chen, W. Liu, Y. Zhang, D. Liu, C. Zhou, S. Shi, J. Dong, Z. Lai, B. Zhao, W. Zhang, H. Cheng, S. Li, TIMEDB: Tumor immune micro-environment cell composition database with automatic analysis and interactive visualization. *Nucleic Acids Res.* **51**, D1417–D1424 (2023).
62. T. C. Brown, J. Jiricny, Repair of base-base mismatches in simian and human cells. *Genome* **31**, 578–583 (1989).
63. M. Haruna, A. Ueyama, Y. Yamamoto, M. Hirata, K. Goto, H. Yoshida, N. Higuchi, T. Yoshida, Y. Kidani, Y. Nakamura, M. Nagira, A. Kawashima, K. Iwahori, Y. Shintani, N. Ohkura, H. Wada, The impact of CCR8+ regulatory T cells on cytotoxic T cell function in human lung cancer. *Sci. Rep.* **12**, 5377 (2022).
64. T. Wang, Q. Zhou, H. Zeng, H. Zhang, Z. Liu, J. Shao, Z. Wang, Y. Xiong, J. Wang, Q. Bai, Y. Xia, Y. Wang, L. Liu, Y. Zhu, L. Xu, B. Dai, J. Guo, Y. Chang, X. Wang, J. Xu, CCR8 blockade primes anti-tumor immunity through intratumoral regulatory T cells destabilization in muscle-invasive bladder cancer. *Cancer Immunol. Immunother.* **69**, 1855–1867 (2020).
65. E. Righi, S. Kashiwagi, J. Yuan, M. Santosuosso, P. Leblanc, R. Ingraham, B. Forbes, B. Edelblute, B. Collette, D. Xing, M. Kowalski, M. C. Mingari, F. Vianello, M. Birrer, S. Orsulic, G. Dranoff, M. C. Poznansky, CXCL12/CXCR4 blockade induces multimodal antitumor effects that prolong survival in an immunocompetent mouse model of ovarian cancer. *Cancer Res.* **71**, 5522–5534 (2011).
66. S. Santagata, M. Napolitano, C. D'Alterio, S. Desicato, S. D. Maro, L. Marinelli, A. Fragale, M. Buoncervello, F. Persico, L. Gabriele, E. Novellino, N. Longo, S. Pignata, S. Perdona, S. Scala, Targeting CXCR4 reverts the suppressive activity of T-regulatory cells in renal cancer. *Oncotarget* **8**, 77110–77120 (2017).
67. Y. Zeng, B. Li, Y. Liang, P. M. Reeves, X. Qu, C. Ran, Q. Liu, M. V. Callahan, A. E. Sluder, J. A. Gelfand, H. Chen, M. C. Poznansky, Dual blockade of CXCL12-CXCR4 and PD-1-PD-L1 pathways prolongs survival of ovarian tumor-bearing mice by prevention of immunosuppression in the tumor microenvironment. *FASEB J.* **33**, 6596–6608 (2019).
68. M. Xydia, R. Rahbari, E. Ruggiero, I. Macaulay, M. Tarabichi, R. Lohmayer, S. Wilkening, T. Michels, D. Brown, S. Vanuytven, S. Mastitskaya, S. Laidlaw, N. Grabe, M. Pritsch, R. Fronza, K. Hexel, S. Schmitt, M. Muller-Steinhardt, N. Halama, C. Domschke, M. Schmidt, C. von Kalle, F. Schutz, T. Voet, P. Beckhove, Common clonal origin of conventional T cells and induced regulatory T cells in breast cancer patients. *Nat. Commun.* **12**, 1119 (2021).
69. H. Kennecke, R. Yerushalmi, R. Woods, M. C. Cheang, D. Voduc, C. H. Speers, T. O. Nielsen, K. Gelmon, Metastatic behavior of breast cancer subtypes. *J. Clin. Oncol.* **28**, 3271–3277 (2010).
70. N. A. Soliman, S. M. Yussif, Ki-67 as a prognostic marker according to breast cancer molecular subtype. *Cancer Biol. Med.* **13**, 496–504 (2016).
71. A. C. Wolff, M. E. H. Hammond, K. H. Allison, B. E. Harvey, P. B. Mangu, J. M. S. Bartlett, M. Bilous, I. O. Ellis, P. Fitzgibbons, W. Hanna, R. B. Jenkins, M. F. Press, P. A. Spears, G. H. Vance, G. Viale, L. M. McShane, M. Dowsett, Human epidermal growth factor receptor 2 testing in breast cancer: American Society of Clinical Oncology/College of American Pathologists clinical practice guideline focused update. *J. Clin. Oncol.* **36**, 2105–2122 (2018).
72. A. Raugh, D. Allard, M. Bettini, Nature vs. nurture: FOXP3, genetics, and tissue environment shape Treg function. *Front. Immunol.* **13**, 911151 (2022).
73. W. A. Woodward, M. S. Chen, F. Behbod, M. P. Alfaro, T. A. Buchholz, J. M. Rosen, WNT/beta-catenin mediates radiation resistance of mouse mammary progenitor cells. *Proc. Natl. Acad. Sci. U.S.A.* **104**, 618–623 (2007).
74. C. Yoon, J. Lu, B. C. Yi, K. K. Chang, M. C. Simon, S. Ryeom, S. S. Yoon, PI3K/Akt pathway and Nanog maintain cancer stem cells in sarcomas. *Oncogenesis* **10**, 12 (2021).
75. Y. Xu, X. Dong, P. Qi, Y. Ye, W. Shen, L. Leng, L. Wang, X. Li, X. Luo, Y. Chen, P. Sun, R. Xiang, N. Li, Sox2 communicates with Tregs through CCL1 to promote the stemness property of breast cancer cells. *Stem Cells* **35**, 2351–2365 (2017).
76. Y. Xu, J. Mou, Y. Wang, W. Zhou, Q. Rao, H. Xing, Z. Tian, K. Tang, M. Wang, J. Wang, Regulatory T cells promote the stemness of leukemia stem cells through IL10 cytokine-related signaling pathway. *Leukemia* **36**, 403–415 (2022).
77. L. Wang, C. Liang, F. Li, D. Guan, X. Wu, X. Fu, A. Lu, G. Zhang, PARP1 in carcinomas and PARP1 inhibitors as antineoplastic drugs. *Int. J. Mol. Sci.* **18**, 2111 (2017).
78. N. McGranahan, A. J. Furness, R. Rosenthal, S. Ramskov, R. Lyngaa, S. K. Saini, M. Jamal-Hanjani, G. A. Wilson, N. J. Birkbak, C. T. Hiley, T. B. Watkins, S. Shafi, N. Murugaesu, R. Mitter, A. U. Akarca, J. Linares, T. Marafioti, J. Y. Henry, E. M. Van Allen, D. Miao, B. Schilling, D. Schadendorf, L. A. Garraway, V. Makarov, N. A. Rizvi, A. Snyder, M. D. Hellmann, T. Merghoub, J. D. Wolchok, S. A. Shukla, C. J. Wu, K. S. Peggs, T. A. Chan, S. R. Hadrup, S. A. Quezada, C. Swanton, Clonal neoantigens elicit T cell immunoreactivity and sensitivity to immune checkpoint blockade. *Science* **351**, 1463–1469 (2016).
79. A. Glaviano, A. S. C. Foo, H. Y. Lam, K. C. H. Yap, W. Jacot, R. H. Jones, H. Eng, M. G. Nair, P. Makvandi, B. Geoerger, M. H. Kulke, R. D. Baird, J. S. Prabhu, D. Carbone, C. Pecoraro, D. B. L. Teh, G. Sethi, V. Cavalieri, K. H. Lin, N. R. Javidi-Sharifi, E. Toska, M. S. Davids, J. R. Brown, P. Diana, J. Stebbing, D. A. Fruman, A. P. Kumar, PI3K/AKT/mTOR signaling transduction pathway and targeted therapies in cancer. *Mol. Cancer* **22**, 138 (2023).
80. P. M. K. Westcott, F. Muyas, H. Hauck, O. C. Smith, N. J. Sacks, Z. A. Ely, A. M. Jaeger, W. M. Rideout III, D. Zhang, A. Bhutkar, M. C. Beytagh, D. A. Canner, G. C. Jaramillo, R. T. Bronson, S. Naranjo, A. Jin, J. J. Patten, A. M. Cruz, S. L. Shanahan, I. Cortes-Ciriano, T. Jacks, Mismatch repair deficiency is not sufficient to elicit tumor immunogenicity. *Nat. Genet.* **55**, 1686–1695 (2023).
81. R. D. Schreiber, L. J. Old, M. J. Smyth, Cancer immunoediting: Integrating immunity's roles in cancer suppression and promotion. *Science* **331**, 1565–1570 (2011).
82. M. Efremova, F. Finotello, D. Rieder, Z. Trajanoski, Neoantigens generated by individual mutations and their role in cancer immunity and immunotherapy. *Front. Immunol.* **8**, 1679 (2017).
83. P. Baldominos, A. Barbera-Mourelle, O. Barreiro, Y. Huang, A. Wight, J. W. Cho, X. Zhao, G. Estivill, I. Adam, X. Sanchez, S. McCarthy, J. Schaller, Z. Khan, A. Ruzo, R. Pastorello,

E. T. Richardson, D. Dillon, P. Montero-Llopis, R. Barroso-Sousa, J. Forman, S. A. Shukla, S. M. Tolaney, E. A. Mittendorf, U. H. von Andrian, K. W. Wucherpfennig, M. Hemberg, J. Agudo, Quiescent cancer cells resist T cell attack by forming an immunosuppressive niche. *Cell* **185**, 1694–1708.e19 (2022).
84. S. Adams, M. Othus, S. P. Patel, K. D. Miller, R. Chugh, S. M. Schuetze, M. D. Chamberlin, B. J. Haley, A. M. V. Storniolo, M. P. Reddy, S. A. Anderson, C. T. Zimmerman, A. P. O'Dea, H. R. Mirshahidi, J. R. Ahnert, F. J. Brescia, O. Hahn, J. M. Raymond, D. D. Biggs, R. M. Connolly, E. Sharon, L. A. Korde, R. J. Gray, E. Mayerson, M. Plets, C. D. Blanke, Y. K. Chae, R. Kurzrock, A multicenter phase II trial of ipilimumab and nivolumab in unresectable or metastatic metaplastic breast cancer: Cohort 36 of dual anti-CTLA-4 and anti-PD-1 blockade in rare tumors (DART, SWOG S1609). *Clin. Cancer Res.* **28**, 271–278 (2022).
85. R. N. Amaria, S. M. Reddy, H. A. Tawbi, M. A. Davies, M. I. Ross, I. C. Glitza, J. N. Cormier, C. Lewis, W. J. Hwu, E. Hanna, A. Diab, M. K. Wong, R. Royal, N. Gross, R. Weber, S. Y. Lai, R. Ehlers, J. Blando, D. R. Milton, S. Woodman, R. Kageyama, D. K. Wells, P. Hwu, S. P. Patel, A. Lucci, A. Hessel, J. E. Lee, J. Gershenwald, L. Simpson, E. M. Burton, L. Posada, L. Haydu, L. Wang, S. Zhang, A. J. Lazar, C. W. Hudgens, V. Gopalakrishnan, A. Reuben, M. C. Andrews, C. N. Spencer, V. Prieto, P. Sharma, J. Allison, M. T. Tetzlaff, J. A. Wargo, Neoadjuvant immune checkpoint blockade in high-risk resectable melanoma. *Nat. Med.* **24**, 1649–1654 (2018).
86. M. D. Hellmann, T. E. Ciuleanu, A. Pluzanski, J. S. Lee, G. A. Otterson, C. Audigier-Valette, E. Minenza, H. Linardou, S. Burgers, P. Salman, H. Borghaei, S. S. Ramalingam, J. Brahmer, M. Reck, K. J. O'Byrne, W. J. Geese, G. Green, H. Chang, J. Szustakowski, P. Bhagavatheeswaran, D. Healey, Y. Fu, F. Nathan, L. Paz-Ares, Nivolumab plus ipilimumab in lung cancer with a high tumor mutational burden. *N. Engl. J. Med.* **378**, 2093–2104 (2018).
87. J. A. Kyte, N. K. Andresen, H. G. Russnes, S. O. Fretland, R. S. Falk, O. C. Lingjaerde, B. Naume, ICON: A randomized phase IIb study evaluating immunogenic chemotherapy combined with ipilimumab and nivolumab in patients with metastatic hormone receptor positive breast cancer. *J. Transl. Med.* **18**, 269 (2020).
88. A. Ribas, J. D. Wolchok, Cancer immunotherapy using checkpoint blockade. *Science* **359**, 1350–1355 (2018).
89. Z. Zhang, Y. Yu, Z. Zhang, D. Li, Z. Liang, L. Wang, Y. Chen, Y. Liang, H. Niu, Cancer-associated fibroblasts-derived CXCL12 enhances immune escape of bladder cancer through inhibiting P62-mediated autophagic degradation of PDL1. *J. Exp. Clin. Cancer Res.* **42**, 316 (2023).
90. D. Hu, Z. Li, B. Zheng, X. Lin, Y. Pan, P. Gong, W. Zhuo, Y. Hu, C. Chen, L. Chen, J. Zhou, L. Wang, Cancer-associated fibroblasts in breast cancer: Challenges and opportunities. *Cancer Commun (Lond)* **42**, 401–434 (2022).
91. D. P. Anastasiadou, A. Quesnel, C. L. Duran, P. S. Filippou, G. S. Karagiannis, An emerging paradigm of CXCL12 involvement in the metastatic cascade. *Cytokine Growth Factor Rev.* **75**, 12–30 (2024).
92. C. W. Elston, I. O. Ellis, Pathological prognostic factors in breast cancer. I. The value of histological grade in breast cancer: Experience from a large study with long-term follow-up. *Histopathology* **19**, 403–410 (1991).
93. P. H. Tan, I. Ellis, K. Allison, E. Brogi, S. B. Fox, S. Lakhani, A. J. Lazar, E. A. Morris, A. Sahin, R. Salgado, A. Sapino, H. Sasano, S. Schnitt, C. Sotiriou, P. van Diest, V. A. White, D. Lokuhetty, I. A. Cree, WHO Classification of Tumours Editorial Board, The 2019 World Health Organization classification of tumours of the breast. *Histopathology* **77**, 181–185 (2020).
94. W. J. Kent, C. W. Sugnet, T. S. Furey, K. M. Roskin, T. H. Pringle, A. M. Zahler, D. Haussler, The human genome browser at UCSC. *Genome Res.* **12**, 996–1006 (2002).
95. C. Fresno, E. A. Fernandez, RDAVIDWebService: A versatile R interface to DAVID. *Bioinformatics* **29**, 2810–2811 (2013).
96. W. Walter, F. Sanchez-Cabo, M. Ricote, GOplot: An R package for visually combining expression data with functional analysis. *Bioinformatics* **31**, 2912–2914 (2015).
97. G. Yu, L. G. Wang, Y. Han, Q. Y. He, clusterProfiler: An R package for comparing biological themes among gene clusters. *OMICS* **16**, 284–287 (2012).
98. A. Colaprico, T. C. Silva, C. Olsen, L. Garofano, C. Cava, D. Garolini, T. S. Sabedot, T. M. Malta, S. M. Pagnotta, I. Castiglioni, M. Ceccarelli, G. Bontempi, H. Noushmehr, TCGAbiolinks: An R/Bioconductor package for integrative analysis of TCGA data. *Nucleic Acids Res.* **44**, e71 (2016).
99. A. Mayakonda, D. C. Lin, Y. Assenov, C. Plass, H. P. Koeffler, Maftools: Efficient and comprehensive analysis of somatic variants in cancer. *Genome Res.* **28**, 1747–1756 (2018).
100. M. S. Lawrence, P. Stojanov, P. Polak, G. V. Kryukov, K. Cibulskis, A. Sivachenko, S. L. Carter, C. Stewart, C. H. Mermel, S. A. Roberts, A. Kiezun, P. S. Hammerman, A. McKenna, Y. Drier, L. Zou, A. H. Ramos, T. J. Pugh, N. Stransky, E. Helman, J. Kim, C. Sougnez, L. Ambrogio, E. Nickerson, E. Shefler, M. L. Cortes, D. Auclair, G. Saksena, D. Voet, M. Noble, D. DiCara, P. Lin, L. Lichtenstein, D. I. Heiman, T. Fennell, M. Imielinski, B. Hernandez, E. Hodis, S. Baca, A. M. Dulak, J. Lohr, D. A. Landau, C. J. Wu, J. Melendez-Zajgla, A. Hidalgo-Miranda, A. Koren, S. A. McCarroll, J. Mora, B. Crompton, R. Onofrio, M. Parkin, W. Winckler, K. Ardlie, S. B. Gabriel, C. W. M. Roberts, J. A. Biegel, K. Stegmaier, A. J. Bass, L. A. Garraway, M. Meyerson, T. R. Golub, D. A. Gordenin, S. Sunyaev, E. S. Lander, G. Getz, Mutational heterogeneity in cancer and the search for new cancer-associated genes. *Nature* **499**, 214–218 (2013).
101. R. Gaujoux, C. Seoighe, A flexible R package for nonnegative matrix factorization. *BMC Bioinformatics* **11**, 367 (2010).
102. V. Thorsson, D. L. Gibbs, S. D. Brown, D. Wolf, D. S. Bortone, T. H. Ou Yang, E. Porta-Pardo, G. F. Gao, C. L Plaisier, J. A. Eddy, E. Ziv, A. C. Culhane, E. O. Paull, I. K. A. Sivakumar, A. J. Gentles, R. Malhotra, F. Farshidfar, A. Colaprico, J. S. Parker, L. E. Mose, N. S. Vo, J. Liu, Y. Liu, J. Rader, V. Dhankani, S. M. Reynolds, R. Bowlby, A. Califano, A. D. Cherniack, D. Anastassiou, D. Bedognetti, Y. Mokrab, A. M. Newman, A. Rao, K. Chen, A. Krasnitz, H. Hu, T. M. Malta, H. Noushmehr, C. S. Pedamallu, S. Bullman, A. I. Ojesina, A. Lamb, W. Zhou, H. Shen, T. K. Choueiri, J. N. Weinstein, J. Guinney, J. Saltz, R. A. Holt, C. S. Rabkin, Cancer Genome Atlas Research Network, A. J. Lazar, J. S. Serody, E. G. Demicco, M. L. Disis, B. G. Vincent, I. Shmulevich, The Immune Landscape of Cancer. *Immunity* **51**, 411–412 (2019); https://doi.org/10.1016/j.immuni.2019.08.004.

Acknowledgments: We thank the study participants of this study, M. Montagna e Salvatore De Simone for technical support, and G. Criscuolo and R. Poto for critical reading of the manuscript. I.C. acknowledges support by Fondazione Italiana Sclerosi Multipla (FISM) cod.2020/BC/001 and financed or cofinanced with the "5 per mille" public funding. A.L. acknowledges support by Fondazione Umberto Veronesi. A.Pe. acknowledges support by the University Research Funding Program (FRA) 2022 of the University of Naples "Federico II." **Funding:** This work was supported by grants from Fondazione Italiana Sclerosi Multipla (2018/R/4), Ministry of Education, University and Research (MIUR) PRIN 2022KT2HBJ, PRIN-PNRR 2022C5KBT, European Union - Next Generation EU "PE8 Ageing Well in an ageing society – AGE-IT" Investment 1.3 (Partenariato Esteso - PE0000015) and Associazione Italiana per la Ricerca sul Cancro-TRIDEO (Transforming Ideas in Oncological research, n.17447) to V.D.R. **Author contributions:** Conceptualization: V.D.R., I.C., and A.Pe. Data curation: B.D.S., A.Pe., T.M., A.L.F., G.T.M., V.D.R., F.D.R., C.F., A.A., I.D., A.C., and E.E. Formal analysis: L.I., B.D.S., A.Pe., T.M., A.Po., G.T.M., V.D.R., F.D.R., C.F., A.A., A.C., V.G., M.M., B.Z., and M.d.B. Funding acquisition: V.D.R., I.C., A. Pe., and G.M. Investigation: L.I., B.D.S., A.Pe., T.M., A.L.F., A.Po., G.T.M., V.D.R., F.D.R., M.P., C.F., A.A., I.D., A.F., F.C., A.C., and E.E. Methodology: G.M., B.D.S., A.Pe., T.M., G.T.M., V.D.R., F.D.R., C.F., A.A., A.F., A.C., and D.R. Project administration: V.D.R., I.C., and A.Pe. Resources: L.I., I.C., G.M., B.D.S., A.Pe., A.L.F., A.Po., F.P., G.T.M., V.D.R., M.P., A.A., A.F., F.G., F.C., E.E., V.G., M.M., B.Z., and M.d.B. Software: B.D.S., A.Pe., G.T.M., M.P., A.A., and I.D. Supervision: G.M., A.Pe., G.T.M., V.D.R., F.D.R., A.A., and E.E. Validation: A.L., I.C., G.M., B.D.S., A.Pe., T.M., G.T.M., V.D.R., F.D.R., C.F., A.A., I.D., A.F., F.C., A.C., and D.R. Visualization: A.L., L.I., I.C., A.S., B.D.S., A.Pe., T.M., G.T.M., V.D.R., F.D.R., C.F., A.A., A.F., F.C., A.C., E.E., and D.R. Writing—original draft: A.L., G.V., I.C., B.D.S., A.Pe., G.T.M., V.D.R., F.D.R., and A.A. Writing—review and editing: A.L., G.V., I.C., B.D.S., A.Pe., G.T.M., F.D.R., M.P., A.A., E.E., and D.R. **Competing interests:** The authors declare that they have no competing interests. **Data and materials availability:** All data needed to evaluate the conclusions in the paper are present in the paper and/or the Supplementary Materials. This study used data from TCGA pilot project established by NCI and the National Human Genome Research Institute, partly via public repositories and partly via the Genotypes and Phenotypes Authorization Database (dbGaP) (accession number: phs000178.v11.p8). Links to public repositories can be found via online citations.

Submitted 16 July 2024
Accepted 13 December 2024
Published 15 January 2025
10.1126/sciadv.adr7934